THE EUROPEAN
PHYSICAL JOURNAL C

Testing lepton flavour universality with (semi)-leptonic $D_{(s)}$ decays

Robert Fleischer[1,2], **Ruben Jaarsma**[1], **Gabriël Koole**[1,3,a]

[1] Nikhef, Science Park 105, 1098 XG Amsterdam, The Netherlands
[2] Faculty of Science, Vrije Universiteit Amsterdam, 1081 HV Amsterdam, The Netherlands
[3] Max Planck Institute for Physics, Föhringer Ring 6, 80805 Munich, Germany

Abstract Data in B-meson decays indicate violations of lepton flavour universality, thereby raising the question about such phenomena in the charm sector. We perform a model-independent analysis of NP contributions in (semi)-leptonic decays of $D_{(s)}$ mesons which originate from $c \to d\bar{\ell}\nu_l$ and $c \to s\bar{\ell}\nu_\ell$ charged-current interactions. Starting from the most general low-energy effective Hamiltonian containing four-fermion operators and the corresponding short-distance coefficients, we explore the impact of new (pseudo)-scalar, vector and tensor operators and constrain their effects through the interplay with current data. We pay special attention to the elements $|V_{cd}|$ and $|V_{cs}|$ of the Cabibbo–Kobayashi–Maskawa matrix and extract them from the $D_{(s)}$ decays in the presence of possible NP decay contributions, comparing them with determinations utilizing unitarity. We find a picture in agreement with the Standard Model within the current uncertainties. Using the results from our analysis, we make also predictions for leptonic $D_{(s)}^+ \to e^+\nu_e$ modes which could be hugely enhanced with respect to their tiny Standard Model branching ratios. It will be interesting to apply our strategy at the future high-precision frontier.

1 Introduction

Forty-five years after the discovery of the charm quark, flavour physics has developed into a broad line of research, allowing us to probe the Standard Model (SM) with unprecedented sensitivity to new interactions and particles at energy scales far beyond the TeV regime which is directly accessible at the Large Hadron Collider (LHC) today [1].

In these explorations, decays of B mesons usually play the key role. Measurements by the BaBar, Belle and LHCb collaborations of processes originating from $b \to c\ell^-\bar{\nu}_\ell$ and $b \to s\ell^+\ell^-$ quark-level transitions indicate deviations from

the SM, where the following observables are in the focus ($\ell = e, \mu$):

$$\mathcal{R}_{D^{(*)}} \equiv \frac{\mathcal{B}(B \to D^{(*)}\tau^-\nu_\tau)}{\mathcal{B}(B \to D^{(*)}\ell^-\nu_\ell)}, \quad R_{K^{(*)}} \equiv \frac{\mathcal{B}(B \to K^{(*)}\mu^+\mu^-)}{\mathcal{B}(B \to K^{(*)}e^+e^-)}. \tag{1}$$

The experimental values of these ratios show tensions with respect to the corresponding SM predictions at the (2–3)σ level (for recent reviews, see, e.g., Refs. [2,3]). In particular, the data raise the exciting question of a possible violation of a central feature of the SM: lepton flavour universality (LFU).

On the theory side, various models of New Physics (NP), i.e. physics lying beyond the SM, have been proposed that could explain the B-decay anomalies, allowing in particular also for violations of LFU. Important specific scenarios are given by leptoquark models [7–12], Z' models [13–15] or Two-Higgs-Doublet models [16–18], implying usually a rich phenomenology of patterns and correlations among various observables.

In view of the potential violation of LFU in B-meson decays, it is interesting to search for such phenomena and possible signals of physics beyond the SM also in the charm sector. In fact, in NP scenarios allowing us to describe the B decay anomalies, effects may also arise in weak decay processes of D mesons. In Ref. [19], rare decays of the kind $D \to \pi\ell\ell$ and $D_s \to K\ell\ell$ have recently been analyzed. These modes arise form flavour-changing neutral current (FCNC) interactions and are the counterparts of the rare B decays entering the $R_{K^{(*)}}$ ratios in Eq. (1). Such processes are usually considered as particularly powerful NP probes as they are not allowed in the SM at the tree level but originate from quantum fluctuations at the loop level. For an analysis of rare $s \to d$ kaon processes, see Ref. [20]. However, decays caused by charged-current interactions at the SM tree level may also be affected by NP effects, as indicated by the $\mathcal{R}_{D^{(*)}}$ observables in Eq. (1). This opens up the door to

[a] e-mail: koole@mpp.mpg.de (corresponding author)

investigate such NP effects in the corresponding decays of charmed mesons as well [21].

In this paper, we shall probe LFU violating effects through (semi)-leptonic $D_{(s)}$-meson decays, applying the strategy proposed in Refs. [22,23] for (semi)-leptonic decays of $B_{(s)}$ mesons. Precise lattice QCD calculations and experimental information on leptonic and semileptonic decays of $D_{(s)}$ mesons, arising from $c \to d\bar{\ell}\nu_\ell$ or $c \to s\bar{\ell}\nu_\ell$ quark-level transitions, allow us to test LFU in the charm sector. In particular, we constrain short-distance coefficients describing physics beyond the SM through a comparison of theoretical calculations with experimental data. Furthermore, we will extract the Cabibbo–Kobayashi–Maskawa (CKM) matrix elements $|V_{cd}|$ and $|V_{cs}|$ from weak charm decays, also in the presence of NP contributions, and will make predictions for leptonic $D_{(s)}^+ \to e^+\nu_e$ decays. These modes could be hugely enhanced through new pseudoscalar contributions, in fact close to the current experimental upper bounds on the corresponding branching ratios.

The outline of this paper is as follows: in Sect. 2, we introduce the most general basis of local operators describing (semi)-leptonic $D_{(s)}$ decays, and discuss the resulting low-energy effective Hamiltonian. Furthermore, we exploit the unitarity of the CKM matrix to determine $|V_{cd(s)}|$ without any use of information following from $D_{(s)}$ decay data. In Sect. 3, we utilize current experimental information on leptonic $D_{(s)}$ decays to constrain the short-distance coefficients for NP contributions. Subsequently, in Sect. 4 we perform a similar analysis for semileptonic $D_{(s)}$ decays. In Sect. 5, we use some of the obtained constraints to determine $|V_{cd}|$ and $|V_{cs}|$ in the presence of pseudoscalar NP interactions. In Sect. 6, we discuss predictions for leptonic $D_{(s)}^+ \to e^+\nu_e$ decays. Finally, we present our conclusions and outlook in Sect. 7.

2 Theoretical framework

2.1 Low-energy effective Hamiltonian

The charged-current interaction processes underlying weak decays of $D_{(s)}$ mesons can be described by local four-fermion operators with their associated short-distance Wilson coefficient functions. Considering all possible Lorentz structures for decays originating from $c \to d\bar{\ell}\nu_l$ or $c \to s\bar{\ell}\nu_\ell$ transitions (with $\ell = e, \mu, \tau$) and assuming neutrinos to be left-handed, we obtain the following operator basis (with $q = d, s$) [24,25]:

$$\mathcal{O}_{V_L}^\ell = (\bar{q}_L\gamma_\mu c_L)(\bar{\nu}_{\ell L}\gamma^\mu \ell_L),$$
$$\mathcal{O}_{V_R}^\ell = (\bar{q}_R\gamma_\mu c_R)(\bar{\nu}_{\ell L}\gamma^\mu \ell_L),$$
$$\mathcal{O}_{S_1}^\ell = (\bar{q}_L c_R)(\bar{\nu}_{\ell L}\ell_R),$$

$$\mathcal{O}_{S_2}^\ell = (\bar{q}_R c_L)(\bar{\nu}_{\ell L}\ell_R),$$
$$\mathcal{O}_T^\ell = (\bar{q}_L \sigma^{\mu\nu} c_R)(\bar{\nu}_{\ell L}\sigma_{\mu\nu}\ell_R). \tag{2}$$

The antisymmetric tensor is defined as $\sigma^{\mu\nu} \equiv \frac{i}{2}[\gamma^\mu, \gamma^\nu]$. Using the appropriate Fierz identity, one can show that the tensor operator with opposite quark chiralities vanishes. In our analysis, it will be convenient to switch to an operator basis that contains a single operator describing the scalar interactions and, similarly, a single pseudoscalar operator. To this end, we define the scalar and pseudoscalar operators in the following way:

$$\mathcal{O}_S^\ell \equiv \frac{1}{2}\left(\mathcal{O}_{S_1}^\ell + \mathcal{O}_{S_2}^\ell\right) = \frac{1}{2}(\bar{q}c)(\bar{\nu}_{\ell L}\ell_R),$$
$$\mathcal{O}_P^\ell \equiv \frac{1}{2}\left(\mathcal{O}_{S_1}^\ell - \mathcal{O}_{S_2}^\ell\right) = \frac{1}{2}(\bar{q}\gamma_5 c)(\bar{\nu}_{\ell L}\ell_R). \tag{3}$$

The most general effective Hamiltonian containing all possible local operators of the lowest dimension for $c \to q\bar{\ell}\nu_\ell$ transitions can therefore be written as

$$\mathcal{H}_{\text{eff}} = \frac{4G_F}{\sqrt{2}}V_{cq}\Big[(1 + C_{V_L}^\ell)\mathcal{O}_{V_L}^\ell + C_{V_R}^\ell\mathcal{O}_{V_R}^\ell$$
$$+ C_S^\ell\mathcal{O}_S^\ell + C_P^\ell\mathcal{O}_P^\ell + C_T^\ell\mathcal{O}_T^\ell\Big], \tag{4}$$

where the subscripts V_L, V_R, S, P and T denote the left-handed vector, right-handed vector, scalar, pseudoscalar and tensor contributions, respectively. In the SM, only the left-handed vector operator is present with an overall Wilson coefficient equal to one. In our analysis, we shall assume real Wilson coefficients for simplicity, i.e. that the NP effects do not involve new sources of CP violation. For a discussion of such effects in the analogous B decays, we refer the reader to Refs. [22,23].

2.2 $|V_{cd}|$ and $|V_{cs}|$ from unitarity

The CKM matrix elements V_{cd} and V_{cs} are usually determined directly from leptonic and semileptonic $D_{(s)}$ decays and assuming the SM (such an extraction from experimental D decay rates using lattice QCD form factors was performed in Ref. [26]). In this work, we are investigating these decays in the presence of NP contributions, hence we need an independent determination of V_{cd} and V_{cs}. To this end, we adopt the Wolfenstein parametrization [27] of the CKM matrix, exploiting its unitarity. Here, V_{cd} and V_{cs} are related to the Wolfenstein parameters $\{\lambda, A, \rho, \eta\}$. Including corrections up to $\mathcal{O}(\lambda^5)$ yields the following expressions [28,29]:

$$V_{cd} = -\lambda + \frac{1}{2}A^2\lambda^5[1 - 2(\rho + i\eta)] + \mathcal{O}(\lambda^7), \tag{5}$$

$$V_{cs} = 1 - \frac{1}{2}\lambda^2 - \frac{1}{8}\lambda^4(1 + 4A^2) + \mathcal{O}(\lambda^6). \tag{6}$$

The Wolfenstein parameters entering here can be determined without any information from $D_{(s)}$ decays, which is a very

advantageous feature of the charm system. The parameters λ and A are related to the CKM elements V_{us} and V_{cb}, respectively. The absolute value of V_{us} is determined from the experimental information on kaon decays and assuming the SM. The current average of the results from semileptonic K_S^0, K_L^0 and $K^\pm$ decays, combined with $K \to \mu\nu(\gamma)$ decays, is given as follows [30]:

$$|V_{us}| = 0.2243 \pm 0.0005, \tag{7}$$

where the SM has been assumed. For $|V_{cb}|$, the current world average from exclusive and inclusive semileptonic decays of B mesons to charm takes the following value [30]:

$$|V_{cb}| = A\lambda^2 + \mathcal{O}(\lambda^8) = (42.2 \pm 0.8) \times 10^{-3}; \tag{8}$$

measurements of $|V_{cb}|$ obtained from $\mathcal{B}(B \to D^{(*)}\tau\bar{\nu})$ are not included. To determine the remaining Wolfenstein parameters, we further exploit the unitarity of the CKM matrix. The side R_b of the unitarity triangle (UT) of the CKM matrix together with the UT angle γ allows us to determine ρ and η. For the determination of R_b, we use the following current world average for $|V_{ub}|$ obtained from inclusive and exclusive semileptonic B decays assuming the SM [30]:

$$|V_{ub}| = (3.94 \pm 0.36) \times 10^{-3}, \tag{9}$$

combined with the result in Eq. (8). There exist tensions at the 3σ level between the inclusive and exclusive determinations of $|V_{cb}|$ and $|V_{ub}|$ [31]. However, for our analysis, it has an essentially negligible impact as these CKM parameters enter only through strongly suppressed higher-order corrections: $|V_{ub}|$ appears only in the corrections in Eq. (5), which differ from the leading term by four orders of λ. The angle γ is usually determined from the tree-dominated $B \to DK$ decays which yield $\gamma = (73.5^{+4.2}_{-5.1})°$ [30]. However, as possible NP could slightly affect its value, we allow γ to be within $[60°, 80°]$. Varying γ within this range has a very minor impact. Finally, we obtain the following values for $|V_{cd}|$ and $|V_{cs}|$ from the unitarity of the CKM matrix:

$$|V_{cd}| = 0.2242 \pm 0.0005, \tag{10}$$
$$|V_{cs}| = 0.9736 \pm 0.0001. \tag{11}$$

The important feature of these results is that they are independent of possible NP contributions to (semi-)leptonic charged-current charm transitions, which are usually exploited to determine these CKM matrix elements from experimental data. We shall use them as reference values for our analysis discussed below.

3 Leptonic decays

Leptonic $D_{(s)}^+ \to \ell^+\nu_\ell$ decays are the simplest and cleanest weak decay class of charmed mesons. All the hadronic dynamics is captured by a single parameter: the $D_{(s)}$-meson decay constant $f_{D_{(s)}^+}$. Leptonic decays of D and D_s mesons contain the flavour-changing quark transitions $c \to d$ and $c \to s$, respectively. Accurate non-perturbative calculations of the decay constants combined with precise experimental results provide excellent opportunities to perform tests of lepton flavour universality.

In the SM, the branching fraction for leptonic $D_{(s)}^+$ decays is given as

$$\mathcal{B}(D_{(s)}^+ \to \ell^+\nu_\ell)|_{\text{SM}} = \frac{G_F^2}{8\pi}|V_{cq}|^2 f_{D_{(s)}^+}^2 M_{D_{(s)}^+} m_\ell^2 \left(1 - \frac{m_\ell^2}{M_{D_{(s)}^+}^2}\right)^2 \tau_{D_{(s)}^+}, \tag{12}$$

where G_F is Fermi's constant, $\tau_{D_{(s)}^+}$ is the lifetime of the $D_{(s)}^+$ meson, and $M_{D_{(s)}^+}$ and m_ℓ are the masses of the $D_{(s)}^+$ meson and the lepton ($\ell = e, \mu, \tau$), respectively. The decay constants f_{D^+} and $f_{D_s^+}$ are determined from lattice QCD calculations. For our analysis, we use the values determined by the FLAG working group [32]:

$$f_{D^+} = (209.0 \pm 2.4) \text{ MeV}, \tag{13}$$
$$f_{D_s^+} = (248.0 \pm 1.6) \text{ MeV}. \tag{14}$$

The resulting leptonic branching fractions in the SM and their experimental values are given in Table 1. Here, we use the values for $|V_{cd}|$ and $|V_{cs}|$ obtained from unitarity, given in Eqs. (10) and (11), respectively. For the $D_{(s)} \to e^+\nu_e$ decays, only experimental upper bounds are available. This is due to the extremely strong helicity suppression in these processes, which is reflected by the proportionality of the branching fraction to m_ℓ^2. However, potential contributions from pseudoscalar NP interactions could lift the helicity suppression in these decays, thereby making them excellent probes for NP. For previous studies of NP effects in these decays, see Refs. [33–35].

3.1 Constraints on pseudoscalar coefficients

As the scalar contributions coming from $\mathcal{O}_S$ vanish due to parity conservation, we start our NP analysis by considering contributions from new pseudoscalar particles. Using the low-energy effective Hamiltonian in Eq. (4), we complement the SM branching fraction with a pseudoscalar contribution and obtain the following expression:

$$\mathcal{B}(D_{(s)}^+ \to \ell^+\nu_\ell) = \mathcal{B}(D_{(s)}^+ \to \ell^+\nu_\ell)|_{\text{SM}} \left|1 + C_P^\ell \frac{M_{D_{(s)}^+}^2}{m_\ell(m_c + m_q)}\right|^2, \tag{15}$$

where C_P^ℓ is the short-distance coefficient for the pseudoscalar NP contribution, and m_c and m_q are the masses of the charm and down (strange) quarks. In these branching

Table 1 Branching ratios of leptonic D_s^+ decays calculated in the SM and comparison with the currently available experimental values

Decay	SM	Experiment	
$\mathcal{B}(D^+ \to e^+ \nu_e)$	$(9.16 \pm 0.22) \times 10^{-9}$	$< 8.8 \times 10^{-6}$	[30]
$\mathcal{B}(D^+ \to \mu^+ \nu_\mu)$	$(3.89 \pm 0.09) \times 10^{-4}$	$(3.74 \pm 0.17) \times 10^{-4}$	[30]
$\mathcal{B}(D^+ \to \tau^+ \nu_\tau)$	$(1.04 \pm 0.03) \times 10^{-3}$	$(1.20 \pm 0.27) \times 10^{-3}$	[36]
$\mathcal{B}(D_s^+ \to e^+ \nu_e)$	$(1.24 \pm 0.02) \times 10^{-7}$	$< 8.3 \times 10^{-5}$	[30]
$\mathcal{B}(D_s^+ \to \mu^+ \nu_\mu)$	$(5.28 \pm 0.08) \times 10^{-3}$	$(5.50 \pm 0.23) \times 10^{-3}$	[30]
$\mathcal{B}(D_s^+ \to \tau^+ \nu_\tau)$	$(5.15 \pm 0.08) \times 10^{-2}$	$(5.48 \pm 0.23) \times 10^{-2}$	[30]

fractions, the decay constants are the source of the largest theoretical uncertainties. Moreover, they contain the CKM elements $|V_{cd}|$ or $|V_{cs}|$, which we would finally like to determine from these decays, also in the presence of NP contributions. With this in mind, we consider the following ratio of two leptonic decays:

$$R_{\ell_2}^{\ell_1} \equiv \frac{\mathcal{B}(D_{(s)}^+ \to \ell_1^+ \nu_{\ell_1})}{\mathcal{B}(D_{(s)}^+ \to \ell_2^+ \nu_{\ell_2})} = \frac{\alpha^{\ell_1} |1 + \beta^{\ell_1} C_P^{\ell_1}|^2}{\alpha^{\ell_2} |1 + \beta^{\ell_2} C_P^{\ell_2}|^2}, \quad (16)$$

where

$$\alpha^{\ell_{1(2)}} = m_{\ell_{1(2)}}^2 \left(1 - \frac{m_{\ell_{1(2)}}^2}{M_{D_{(s)}^+}^2}\right)^2 \quad \text{and}$$

$$\beta^{\ell_{1(2)}} = \frac{M_{D_{(s)}^+}^2}{[m_{\ell_{1(2)}}(m_c + m_q)]}. \quad (17)$$

This observable is theoretically clean as the decay constants and also the CKM matrix elements cancel.

Let us first consider leptonic decays of D mesons. Using the experimental information in Table 1, we obtain the following value for the ratio between two leptonic D decays with tau leptons and muons in the final state:

$$(R_\mu^\tau)^D = 3.21 \pm 0.73, \quad (18)$$

where we have utilized the recent first observation of the decay $D^+ \to \tau^+ \nu_\tau$ by the BESIII collaboration [36]. By comparing the experimental value with the corresponding theoretical expression, we determine the allowed regions in the C_P^μ–C_P^τ plane. The result is presented in Fig. 1 (left), where the uncertainties coming from the masses are neglected due to their smallness. The SM prediction ($C_P^\mu = C_P^\tau = 0$), indicated by the black star, is in agreement with the obtained constraints at the 1σ level.

For electrons and muons in the final state, we obtain

$$(R_\mu^e)^D < (2.35 \pm 0.11) \times 10^{-2}. \quad (19)$$

Comparison with the corresponding theoretical expression allows us to calculate the allowed regions in the C_P^μ–C_P^e plane. For the branching fraction $\mathcal{B}(D^+ \to e^+ \nu_e)$, only an experimental upper bound is available, resulting in the large wedge-shaped allowed regions in the panel on the right-hand

side of Fig. 1. The SM prediction ($C_P^\mu = C_P^e = 0$) lies within the obtained 1σ contour. A future measurement of $\mathcal{B}(D^+ \to e^+ \nu_e)$ would allow us to determine more stringent constraints in the C_P^μ–C_P^e plane from the $(R_\mu^e)^D$ ratio, in analogy to the constraints following from $(R_\mu^\tau)^D$.

For D_s decays, we perform a similar analysis in the presence of pseudoscalar NP. From the experimental information on leptonic D_s decays in Table 1, we obtain the following value for $(R_\mu^\tau)^{D_s}$:

$$(R_\mu^\tau)^{D_s} = 9.96 \pm 0.59. \quad (20)$$

Using this result, we constrain the corresponding short-distance coefficients. The resulting allowed regions in the C_P^μ–C_P^τ plane are shown in the panel on the left-hand side in Fig. 2. For $(R_\mu^e)^{D_s}$, we obtain the experimental value

$$(R_\mu^e)^{D_s} < (1.51 \pm 0.06) \times 10^{-2}. \quad (21)$$

By comparing our theoretical expression with the experimental information, we obtain the allowed regions in the C_P^μ–C_P^e plane shown in the panel on the right-hand side of Fig. 2. We observe that the obtained 1σ contours for both $(R_\mu^\tau)^{D_s}$ and $(R_\mu^e)^{D_s}$ contain the SM predictions. We would like to note that also for $\mathcal{B}(D_s^+ \to e^+ \nu_e)$, only an experimental upper bound is available. A future measurement of this branching fraction would allow us to put more stringent constraints on the relevant NP coefficients. We shall return to $D_{(s)}^+ \to e^+ \nu_e$ decays in Sect. 6.

3.2 Constraints on vector coefficients

Besides pseudoscalar NP contributions, the SM branching fraction may also be complemented by contributions from additional vector interactions. Including possible left-handed (LH) vector interactions leads to the following branching fraction:

$$\mathcal{B}(D_{(s)}^+ \to \ell^+ \nu_\ell) = \mathcal{B}(D_{(s)}^+ \to \ell^+ \nu_\ell)\big|_{\text{SM}} \left|1 + C_{V_L}^\ell\right|^2, \quad (22)$$

where $C_{V_L}^\ell$ is the short-distance coefficient for the LH vector interaction. Just as for the pseudoscalar coefficients, we need a theoretically clean observable for the extraction of constraints on the vector coefficients. In analogy to Eq. (16),
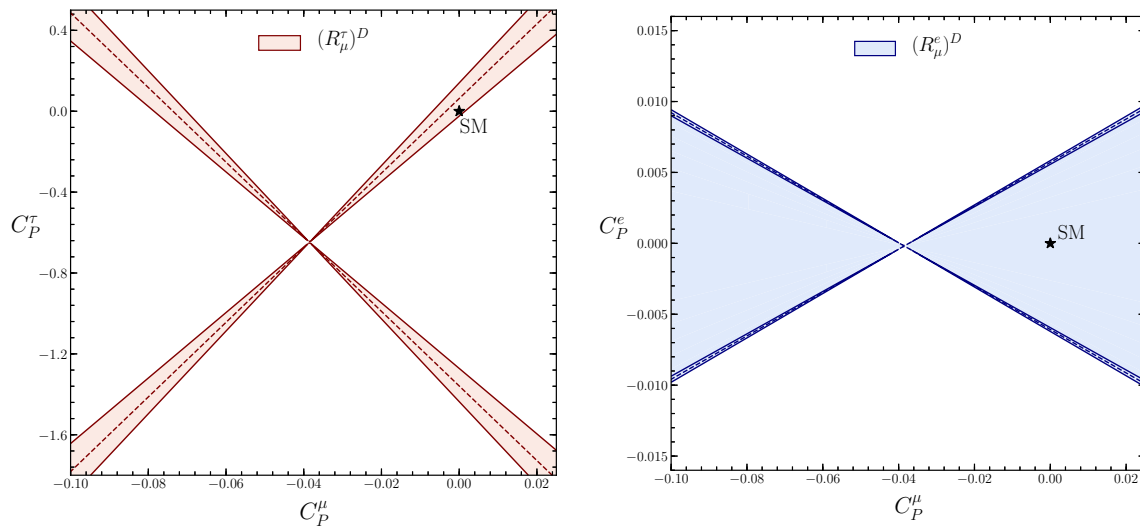
Fig. 1 The allowed regions in the C_P^μ–C_P^τ (left) and C_P^μ–C_P^e (right) planes following from the ratios $(R_\mu^\tau)^D$ and $(R_\mu^e)^D$, respectively. The black stars indicate the SM predictions
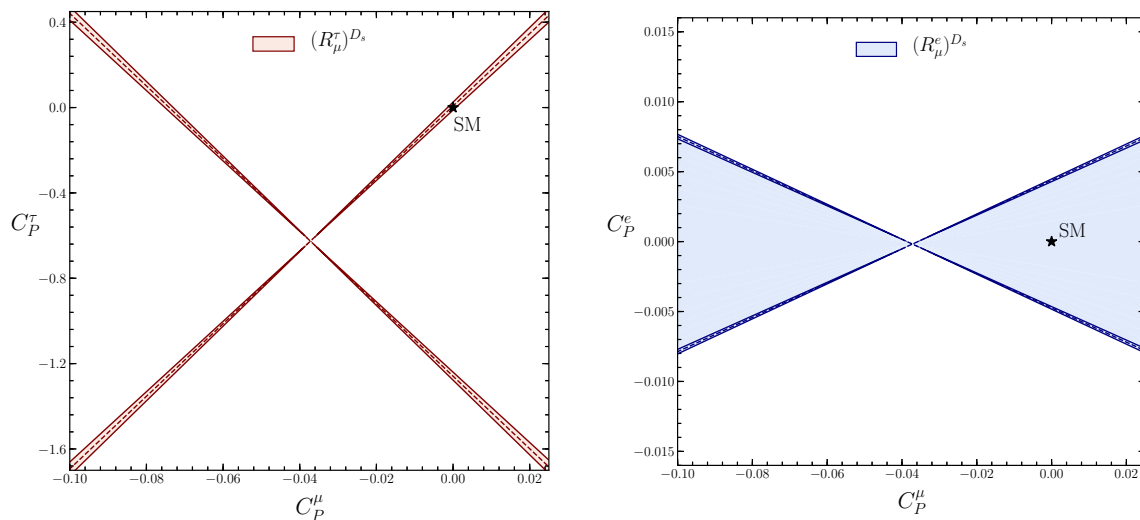

Fig. 2 The allowed regions in the C_P^μ–C_P^τ (left) and C_P^μ–C_P^e (right) planes following from the ratios $(R_\mu^\tau)^{D_s}$ and $(R_\mu^e)^{D_s}$, respectively. The black stars indicate the SM predictions

we define the ratio of two leptonic branching fractions with different leptons in the final state:

$$R_{\ell_2}^{\ell_1} \equiv \frac{\mathcal{B}(D_{(s)}^+ \to \ell_1^+ \nu_{\ell_1})}{\mathcal{B}(D_{(s)}^+ \to \ell_2^+ \nu_{\ell_2})} = \frac{\alpha^{\ell_1} |1 + C_{V_L}^{\ell_1}|^2}{\alpha^{\ell_2} |1 + C_{V_L}^{\ell_2}|^2}. \quad (23)$$

We constrain the LH vector coefficients by comparing the theoretical expressions to the experimental information in Eqs. (18–21). The obtained allowed regions in the $C_{V_L}^\mu$–$C_{V_L}^\tau$ and $C_{V_L}^\mu$–$C_{V_L}^e$ planes are given in Fig. 3.

We proceed our analysis by considering right-handed (RH) vector NP interactions. The branching fraction includ-

ing RH vector contributions takes the following form:

$$\mathcal{B}(D_{(s)}^+ \to \ell^+ \nu_\ell) = \mathcal{B}(D_{(s)}^+ \to \ell^+ \nu_\ell)\big|_{\mathrm{SM}} \Big| 1 - C_{V_R}^\ell \Big|^2, \quad (24)$$

where $C_{V_R}^\ell$ is the short-distance coefficient for the RH vector interaction.

Just as for the LH vector coefficients, we define the ratio of two leptonic branching fractions with different leptons in the final state:

$$R_{\ell_2}^{\ell_1} \equiv \frac{\mathcal{B}(D_{(s)}^+ \to \ell_1^+ \nu_{\ell_1})}{\mathcal{B}(D_{(s)}^+ \to \ell_2^+ \nu_{\ell_2})} = \frac{\alpha^{\ell_1} |1 - C_{V_R}^{\ell_1}|^2}{\alpha^{\ell_2} |1 - C_{V_R}^{\ell_2}|^2}. \quad (25)$$

Using the experimental constraints, we obtain the allowed regions in the $C_{V_R}^\mu$–$C_{V_R}^\tau$ and $C_{V_R}^\mu$–$C_{V_R}^e$ planes shown in Fig. 4.
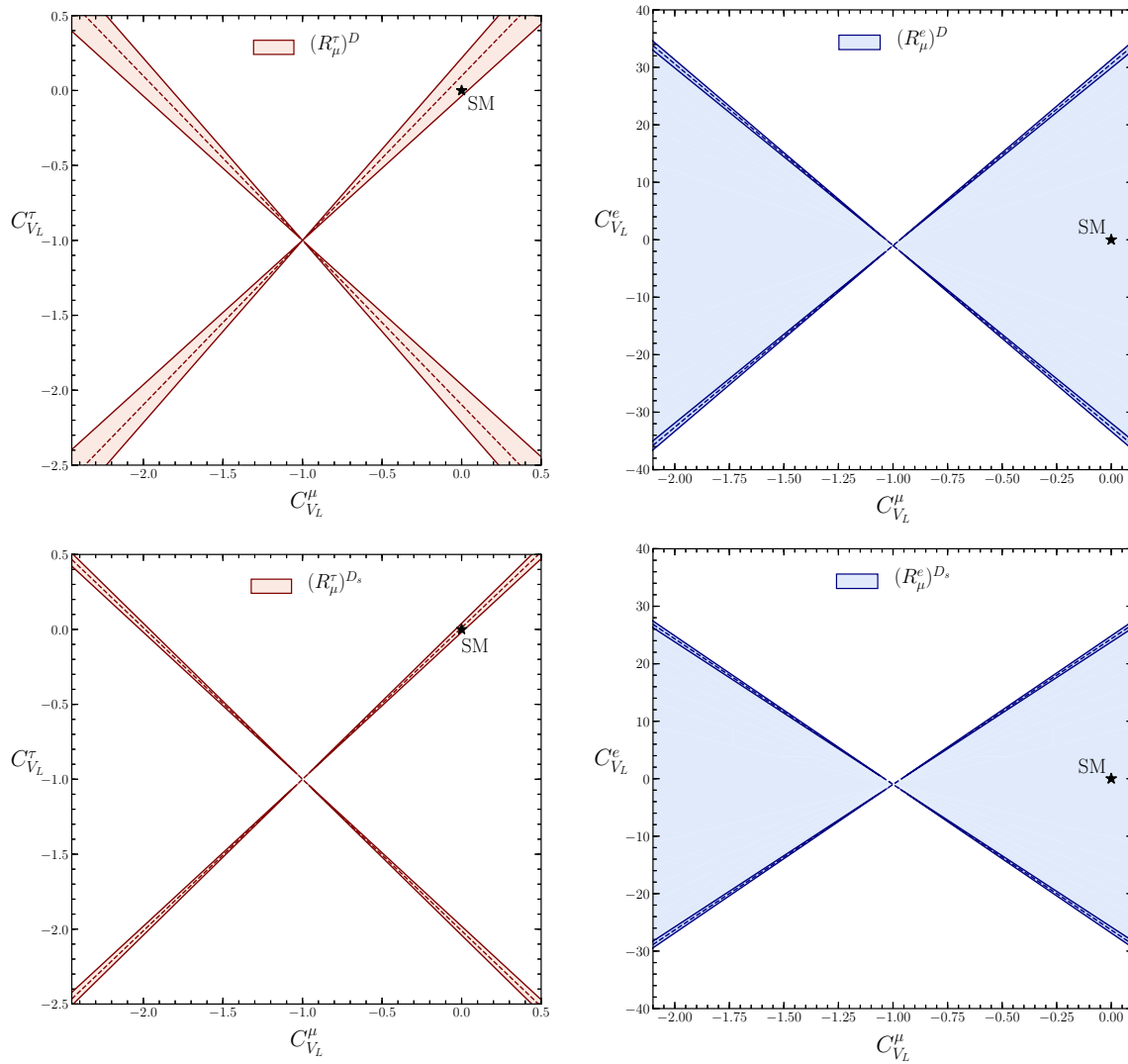
Fig. 3 Allowed regions in the $C_{V_L}^\mu$–$C_{V_L}^\tau$ plane using the ratios $(R_\mu^\tau)^D$ (top left) and $(R_\mu^\tau)^{D_s}$ (bottom left), and in the $C_{V_L}^\mu$–$C_{V_L}^e$ plane using the ratios $(R_\mu^e)^D$ (top right) and $(R_\mu^e)^{D_s}$ (bottom right). The black stars indicate the SM predictions

4 Semileptonic decays

Semileptonic $D_{(s)}$ decays provide further powerful ways to constrain the short-distance NP coefficients. Since they are driven by the same $c \to d\bar{\ell}\nu_\ell$ and $c \to s\bar{\ell}\nu_\ell$ quark transitions, these processes are effectively described by the same local operators. Consequently, constraints on the short-distance coefficients coming from semileptonic decays can be utilized to complement those from leptonic decays.

4.1 $D \to P\bar{\ell}\nu_\ell$ decays

First, we consider the semileptonic D decays of the form $D \to P\bar{\ell}\nu_\ell$, where P denotes a pseudoscalar meson. The differential branching fraction is given in the SM as follows [25]:

$$\frac{d\mathcal{B}(D \to P\bar{\ell}\nu_\ell)}{dq^2}\bigg|_{\text{SM}} = \frac{G_F^2 \tau_D |V_{cq}|^2}{24\pi^3 M_D^2} \left[\frac{(H_{V,0}^P)^2}{4}\left(1 + \frac{m_\ell^2}{2q^2}\right) + \frac{3}{8}\frac{m_\ell^2}{q^2}(H_{V,s}^P)^2 \right]\frac{(q^2 - m_\ell^2)^2}{q^2}|\vec{p}_P|,$$

$$(26)$$

where q^2 is the four-momentum of the lepton-neutrino pair, satisfying the relation

$$m_\ell^2 \leq q^2 \leq (M_D - M_P)^2. \tag{27}$$

In order to calculate the amplitudes $H_{V,0}^P$ and $H_{V,s}^P$, hadronic form factors are needed, requiring non-perturbative methods. In the literature, various form-factor parametrizations were proposed (for a more detailed discussion, see Appendix A). In Table 2, the SM branching fractions for semileptonic $D \to \pi$ and $D \to K$ decays with electrons or muons in the final states

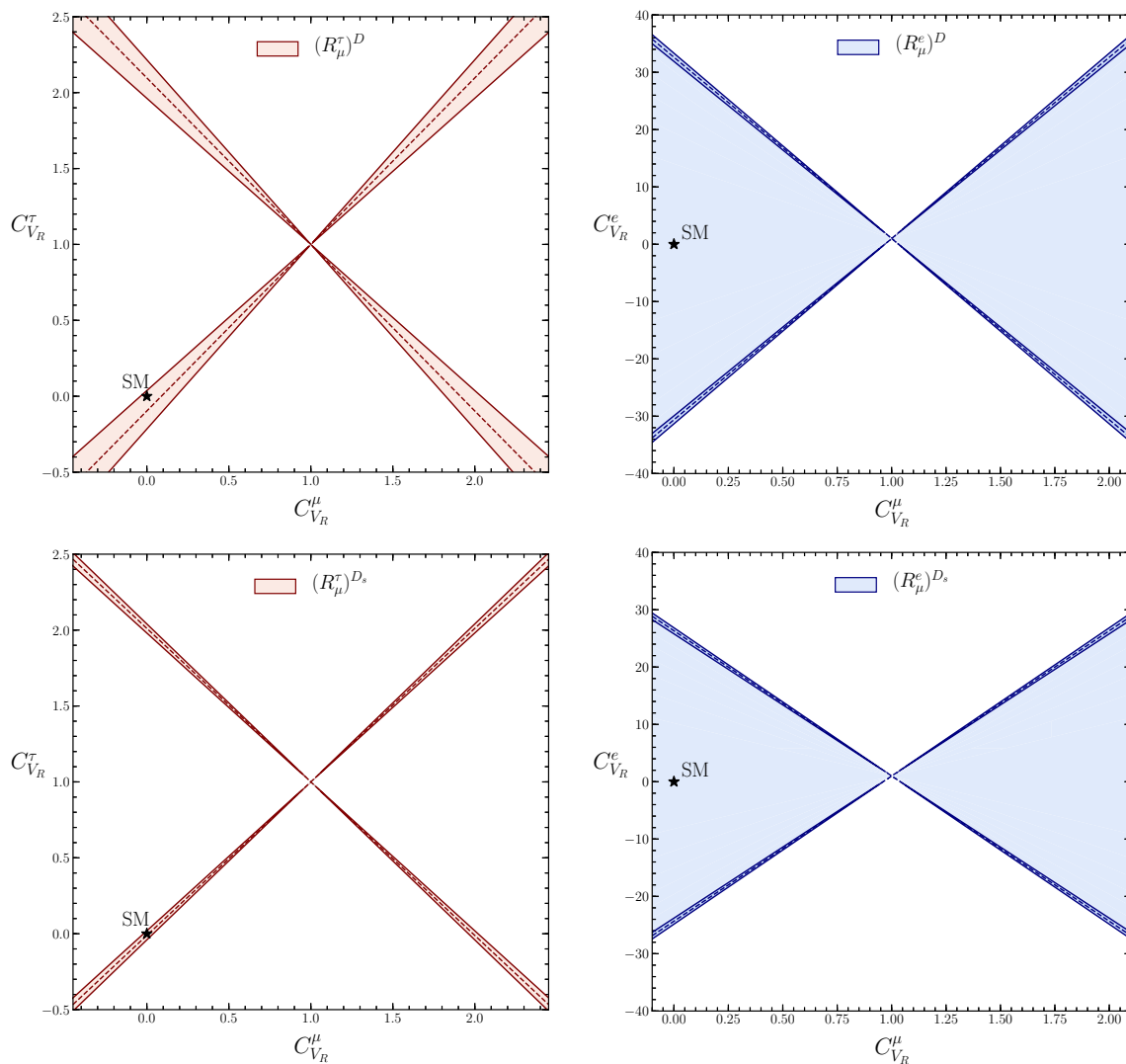**Fig. 4** Allowed regions in the $C_{V_R}^\mu$–$C_{V_R}^\tau$ plane using the ratios $(R_\mu^\tau)^D$ (top left) and $(R_\mu^\tau)^{D_s}$ (bottom left), and in the $C_{V_R}^\mu$–$C_{V_R}^e$ plane using the ratios $(R_\mu^e)^D$ (top right) and $(R_\mu^e)^{D_s}$ (bottom right). The black stars indicate the SM predictions

are given, along with their experimental counterparts. For the SM predictions, we used the values of $|V_{cd}|$ and $|V_{cs}|$ in Eqs. (10) and (11), respectively, obtained from the unitarity of the CKM matrix. Furthermore, we applied the lattice results given in Refs. [37] and [38], adopting double-pole and z-series parametrizations, respectively. As the latter approach results in smaller uncertainties for the branching fractions, we will use it in our analysis outlined below. For a studies using quark model caclulations, we refer the reader to Refs. [40,41].

4.1.1 Constraints on (pseudo)-scalar coefficients

Allowing for scalar NP interactions, the differential branching fraction for semileptonic D decays into a pseudoscalar meson and a lepton–neutrino pair takes the following form:

$$\frac{d\mathcal{B}(D \to P\bar{\ell}\nu_\ell)}{dq^2} = \frac{G_F^2 \tau_D |V_{cq}|^2}{24\pi^3 M_D^2} \left\{ \left[\frac{(H_{V,0}^P)^2}{4} \left(1 + \frac{m_\ell^2}{2q^2}\right) + \frac{3}{8}\frac{m_\ell^2}{q^2}(H_{V,t}^P)^2 \right] \right.$$
$$\left. + \frac{3}{8}|C_S^\ell|^2 (H_S^P)^2 + \frac{3}{4}\mathcal{R}e(C_S^{\ell*})\frac{m_\ell}{\sqrt{q^2}} H_S^P H_{V,t}^P \right\} \frac{(q^2 - m_\ell^2)^2}{q^2}|\vec{p}_P|,$$

(28)

where the term in the square brackets is the SM part. The other terms, containing the NP contributions, are sensitive to the scalar coefficient C_S^ℓ. In order to obtain an observable that is independent of V_{cd} or V_{cs}, we consider the ratio between a leptonic $D_{(s)}$ decay and a semileptonic D decay containing the same quark transition and lepton flavour in the final state. Semileptonic D decays with tau leptons are kinematically forbidden, and for leptonic decays to electrons only an experimental upper bound is available. Therefore, we restrict ourselves to decays with muons in the final state and define

Table 2 Branching fractions for semileptonic D decays calculated in the SM using double-pole [37] and z-series [38] form factor parametrizations, and comparison with the current experimental results given in Ref. [30]

Decay	Double-pole	z-series	Experiment
$\mathcal{B}(D^0 \to \pi^- e^+ \nu_e)$	$(3.21 \pm 0.68) \times 10^{-3}$	$(2.64 \pm 0.31) \times 10^{-3}$	$(2.91 \pm 0.04) \times 10^{-3}$
$\mathcal{B}(D^0 \to K^- e^+ \nu_e)$	$(3.64 \pm 0.76) \times 10^{-2}$	$(3.49 \pm 0.29) \times 10^{-2}$	$(3.542 \pm 0.035) \times 10^{-2}$
$\mathcal{B}(D^+ \to \pi^0 e^+ \nu_e)$	$(4.17 \pm 0.88) \times 10^{-3}$	$(3.42 \pm 0.41) \times 10^{-3}$	$(3.72 \pm 0.17) \times 10^{-3}$
$\mathcal{B}(D^+ \to \overline{K}^0 e^+ \nu_e)$	$(9.31 \pm 1.95) \times 10^{-2}$	$(8.92 \pm 0.75) \times 10^{-2}$	$(8.73 \pm 0.10) \times 10^{-2}$
$\mathcal{B}(D^0 \to \pi^- \mu^+ \nu_\mu)$	$(3.17 \pm 0.67) \times 10^{-3}$	$(2.60 \pm 0.31) \times 10^{-3}$	$(2.67 \pm 0.12) \times 10^{-3}$
$\mathcal{B}(D^0 \to K^- \mu^+ \nu_\mu)$	$(3.56 \pm 0.74) \times 10^{-2}$	$(3.40 \pm 0.29) \times 10^{-2}$	$(3.41 \pm 0.04) \times 10^{-2}$
$\mathcal{B}(D^+ \to \pi^0 \mu^+ \nu_\mu)$	$(4.12 \pm 0.87) \times 10^{-3}$	$(3.38 \pm 0.40) \times 10^{-3}$	$(3.50 \pm 0.15) \times 10^{-3}$
$\mathcal{B}(D^+ \to \overline{K}^0 \mu^+ \nu_\mu)$	$(9.11 \pm 1.90) \times 10^{-2}$	$(8.70 \pm 0.73) \times 10^{-2}$	$(8.76 \pm 0.19) \times 10^{-2}$

the following ratios:

$$\mathcal{R}^\mu_{\mu;\pi^0} \equiv \frac{\mathcal{B}(D^+ \to \mu^+ \nu_\mu)}{\mathcal{B}(D^+ \to \pi^0 \mu^+ \nu_\mu)},$$

$$\mathcal{R}^\mu_{\mu;\pi^-} \equiv \frac{\mathcal{B}(D^+ \to \mu^+ \nu_\mu)}{\mathcal{B}(D^0 \to \pi^- \mu^+ \nu_\mu)}, \tag{29}$$

and

$$\mathcal{R}^\mu_{\mu;\overline{K}^0} \equiv \frac{\mathcal{B}(D_s^+ \to \mu^+ \nu_\mu)}{\mathcal{B}(D^+ \to \overline{K}^0 \mu^+ \nu_\mu)},$$

$$\mathcal{R}^\mu_{\mu;K^-} \equiv \frac{\mathcal{B}(D_s^+ \to \mu^+ \nu_\mu)}{\mathcal{B}(D^0 \to K^- \mu^+ \nu_\mu)}. \tag{30}$$

These observables are sensitive to the scalar and pseudoscalar coefficients C_S^ℓ and C_P^ℓ. For the $D^+ \to \pi^0 \mu^+ \nu_\mu$ decay, an isospin factor of 1/2 has to be taken into account since $\pi^0 = (u\bar{u} - d\bar{d})/\sqrt{2}$. From the measured branching fractions given in Table 2, we obtain the following experimental values:

$$\mathcal{R}^\mu_{\mu;\pi^0} = (1.07 \pm 0.07) \times 10^{-1},$$

$$\mathcal{R}^\mu_{\mu;\pi^-} = (1.40 \pm 0.09) \times 10^{-1}, \tag{31}$$

and

$$\mathcal{R}^\mu_{\mu;\overline{K}^0} = (6.28 \pm 0.30) \times 10^{-2},$$

$$\mathcal{R}^\mu_{\mu;K^-} = (1.61 \pm 0.07) \times 10^{-1}. \tag{32}$$

By comparing the theoretical expressions for the ratios in Eqs. (29) and (30) with the corresponding experimental values, we constrain the (pseudo)-scalar coefficients. From $\mathcal{R}^\mu_{\mu;\pi^0}$ and $\mathcal{R}^\mu_{\mu;\pi^-}$, we obtain the allowed regions in the C_P^μ–C_S^μ plane shown in Fig. 5. The results are in agreement with the SM prediction $C_P^\mu = C_S^\mu = 0$ at the 1σ level. This is also the case for the allowed regions obtained from $\mathcal{R}^\mu_{\mu;\overline{K}^0}$ and $\mathcal{R}^\mu_{\mu;K^-}$, shown in Fig. 6.

4.1.2 Constraints on vector coefficients

Next, we consider contributions from LH and RH vector NP interactions. The differential branching fraction can be written as follows:

$$\frac{d\mathcal{B}(D \to P\bar{\ell}\nu_\ell)}{dq^2} = \frac{d\mathcal{B}(D \to P\bar{\ell}\nu_\ell)}{dq^2}\bigg|_{\text{SM}} \left|1 + C_{V_{L(R)}}^\ell\right|^2. \tag{33}$$

In principle, we could define ratios in analogy to Eqs. (29) and (30) given in the previous section, but include vector contributions instead of (pseudo)-scalar ones. However, Eqs. (22) and (33) indicate that the LH vector NP contributions would cancel. On the other hand, in the case of RH vector contributions, they would not cancel due to the relative sign difference, but the structure of the formulae does prohibit the extraction of stringent constraints.

We can, however, investigate possible vector NP interactions through ratios between two semileptonic decays with different flavours of leptons. To this end, we define the following observables:

$$\mathcal{R}^e_{\mu;\pi^0} \equiv \frac{\mathcal{B}(D^+ \to \pi^0 e^+ \nu_e)}{\mathcal{B}(D^+ \to \pi^0 \mu^+ \nu_\mu)},$$

$$\mathcal{R}^e_{\mu;\pi^-} \equiv \frac{\mathcal{B}(D^0 \to \pi^- e^+ \nu_e)}{\mathcal{B}(D^0 \to \pi^- \mu^+ \nu_\mu)}, \tag{34}$$

and

$$\mathcal{R}^e_{\mu;\overline{K}^0} \equiv \frac{\mathcal{B}(D^+ \to \overline{K}^0 e^+ \nu_e)}{\mathcal{B}(D^+ \to \overline{K}^0 \mu^+ \nu_\mu)},$$

$$\mathcal{R}^e_{\mu;K^-} \equiv \frac{\mathcal{B}(D^0 \to K^- e^+ \nu_e)}{\mathcal{B}(D^0 \to K^- \mu^+ \nu_\mu)}. \tag{35}$$

These observables are independent of CKM matrix elements and sensitive to the coefficients $C_{V_{L(R)}}^\ell$, with $\ell = e, \mu$. Hence, they provide interesting opportunities to test lepton flavour universality in D decays. From the measured branching fractions in Table 2, we obtain the following experimental values:
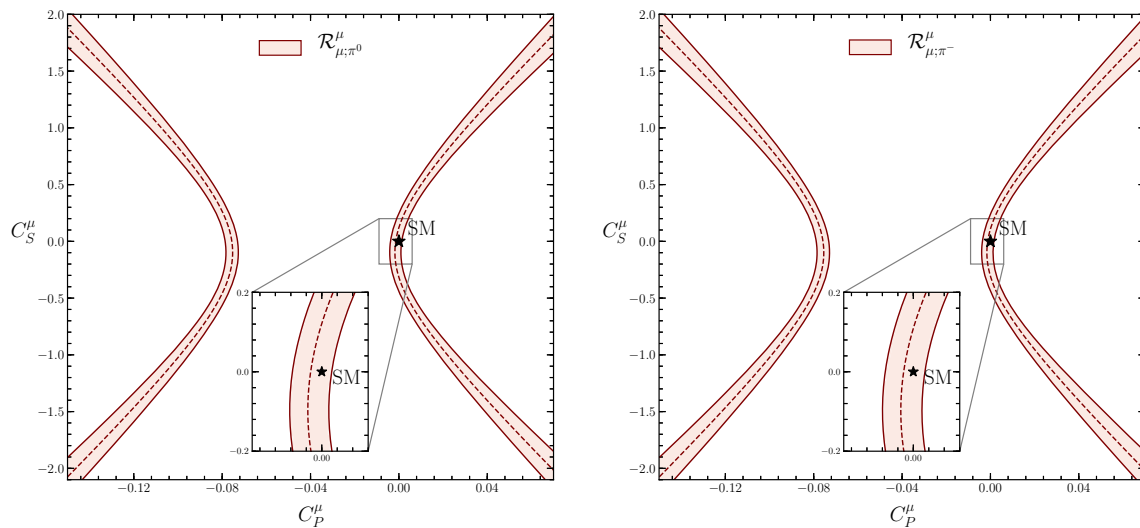
Fig. 5 Allowed regions in the C_P^μ–C_S^μ plane using the ratios $\mathcal{R}_{\mu;\pi^0}^\mu$ (left) and $\mathcal{R}_{\mu;\pi^-}^\mu$ (right)
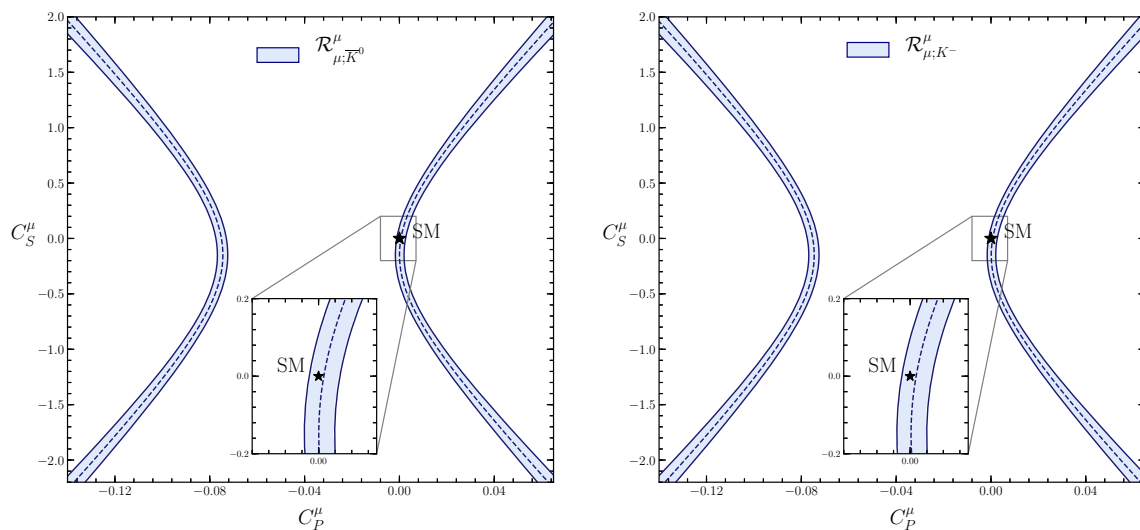

Fig. 6 Allowed regions in the C_P^μ–C_S^μ plane using the ratios $\mathcal{R}_{\mu;\overline{K}^0}^\mu$ (left) and $\mathcal{R}_{\mu;K^-}^\mu$ (right)

$$\mathcal{R}_{\mu;\pi^0}^e = 1.06 \pm 0.07,$$
$$\mathcal{R}_{\mu;\pi^-}^e = 1.09 \pm 0.05, \tag{36}$$

and

$$\mathcal{R}_{\mu;\overline{K}^0}^e = (9.97 \pm 0.24) \times 10^{-1},$$
$$\mathcal{R}_{\mu;K^-}^e = 1.04 \pm 0.01. \tag{37}$$

The structure of the theoretical expressions for these observables, following from Eq. (33), is identical for LH and RH vector NP interactions. Therefore, the allowed regions in the $C_{V_L}^\mu$–$C_{V_L}^e$ and $C_{V_R}^\mu$–$C_{V_R}^e$ planes, obtained by comparing these expression with the experimental values, are the same. This can be seen in Figs. 7 and 8. Furthermore, as leptonic and semileptonic decays are described by the same operators, we

may compare these constraints with the ones obtained from leptonic decays in Figs. 3 (right) and 4 (right). The constraints presented there are a significant improvement, resulting from the fact that semileptonic decays do not suffer from helicity suppression. It is interesting to note that the SM predictions, $C_{V_{L(R)}}^\mu = C_{V_{L(R)}}^e = 0$, lie just outside the 1σ contours in three of the four plots.

4.1.3 Constraints on tensor coefficients

Finally, let us probe the tensor operator in the operator basis given in Eq. (2) through its impact on the semileptonic decays. The differential branching fraction including such tensor interactions is given as
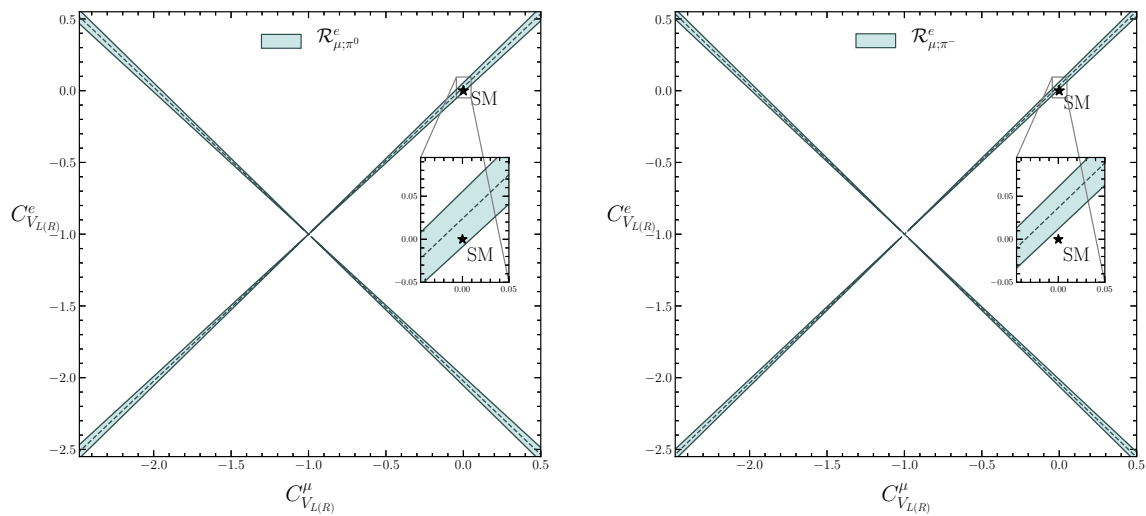
Fig. 7 Allowed regions in the $C^\mu_{V_{L(R)}} - C^e_{V_{L(R)}}$ plane using the ratios $\mathcal{R}^\mu_{\mu;\pi^0}$ (left) and $\mathcal{R}^\mu_{\mu;\pi^-}$ (right)
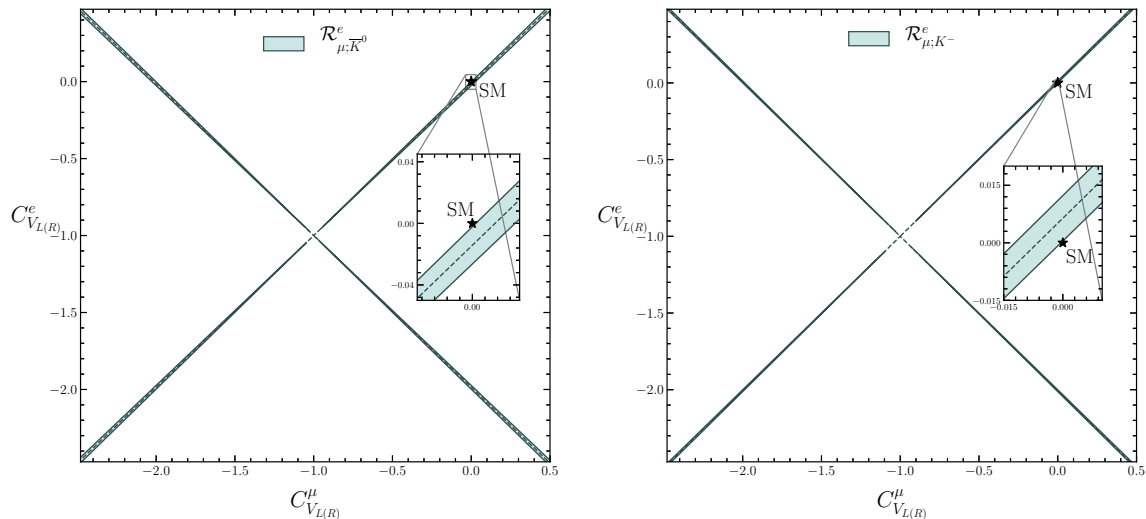

Fig. 8 Allowed regions in the $C^\mu_{V_{L(R)}} - C^e_{V_{L(R)}}$ plane using the ratios $\mathcal{R}^\mu_{\mu;\overline{K}^0}$ (left) and $\mathcal{R}^\mu_{\mu;K^-}$ (right)

$$
\frac{d\mathcal{B}(D \to P\bar\ell\nu_\ell)}{dq^2}
$$
$$
= \frac{G_F^2 \tau_D |V_{cq}|^2}{24\pi^3 M_D^2} \left\{ \left[\frac{(H^P_{V,0})^2}{4}\left(1+\frac{m_\ell^2}{2q^2}\right) + \frac{3}{8}\frac{m_\ell^2}{q^2}(H^P_{V,t})^2 \right] \right.
$$
$$
\left. + 2|C^\ell_T|^2\left(1+\frac{2m_\ell^2}{q^2}\right)(H^P_T)^2 - 3Re(C^{\ell*}_T)\frac{m_\ell}{\sqrt{q^2}}H^P_T H^P_{V,0} \right\}
$$
$$
\frac{(q^2-m_\ell^2)^2}{q^2}|\vec{p}_P|.
$$

$$(38)$$

For the amplitude H^P_T, we use the lattice results obtained in Ref. [39] for the corresponding form factors (for details, see Appendix A). This leads to expressions for the semileptonic branching fractions, dependent on the tensor NP coefficients C^ℓ_T. As the tensor operator in Eq. (2) is antisymmet-

ric in μ and ν, there are no tensor contributions to leptonic decays. Consequently, we cannot probe tensor NP through ratios between leptonic and semileptonic decays. Hence, we take the ratios in Eqs. (34) and (35), but allow for tensor contributions instead of vector contributions. These ratios are then sensitive to the tensor coefficients C^μ_T and C^e_T.

By comparing our theoretical expressions with the experimental information in Eqs. (36) and (37), we determine the allowed regions in the $C^\mu_T - C^e_T$ plane. The constraints from $\mathcal{R}^e_{\mu;\pi^0}$ and $\mathcal{R}^e_{\mu;\pi^-}$ are shown in the panels on the left- and right-hand sides of Fig. 9, respectively. In the latter case, it is interesting to see that the SM prediction corresponding to $C^\mu_T = C^e_T = 0$ is excluded at the 1σ level. In Fig. 10, the allowed regions in the $C^\mu_T - C^e_T$ plane are shown, following from the constraints on $\mathcal{R}^e_{\mu;\overline{K}^0}$ (left) and $\mathcal{R}^e_{\mu;K^-}$ (right). We

observe that in the case of $\mathcal{R}^e_{\mu;\overline{K}^0}$, the SM prediction lies just outside the 1σ contours.

4.2 $D \to V\bar{\ell}\nu_\ell$ decays

We continue our analysis of semileptonic $D_{(s)}$ decays by considering decays of the form $D \to V\bar{\ell}\nu_\ell$, where V denotes a vector meson. Measurements of the branching fractions for $D \to \rho$ and $D \to K^*$ decays allow us to further constrain the short-distance NP coefficients. In particular, $D \to V$ decays are sensitive to the pseudoscalar NP coefficient C_P^ℓ, thereby offering an interesting complement to the constraints following from the leptonic decays in Sect. 3.

The SM expression for the differential branching fraction for $D \to V\bar{\ell}\nu_\ell$ decays takes the form [25]

$$\frac{d\mathcal{B}(D \to V\bar{\ell}\nu_\ell)}{dq^2} = \frac{G_F^2 \tau_D |V_{cq}|^2}{24\pi^3 M_D^2} \left\{ \frac{1}{4}\left(1 + \frac{m_\ell^2}{2q^2}\right)\left[(H_{V,+}^V)^2 \right. \right.$$
$$\left. + (H_{V,-}^V)^2 + (H_{V,0}^V)^2\right] + \frac{3}{8}\frac{m_\ell^2}{q^2}(H_{V,t}^V)^2 \right\} \tag{39}$$
$$\frac{(q^2 - m_\ell^2)^2}{q^2}|\vec{p}_V|,$$

where q^2 has the kinematical range

$$m_\ell^2 \le q^2 \le (M_D - M_V)^2. \tag{40}$$

In comparison with the pseudoscalar case, we have now a considerably more complex situation due to the amplitudes $H_{V,+}^V$, $H_{V,-}^V$, $H_{V,0}^V$ and $H_{V,t}^V$, which involve various hadronic form factors. Unfortunately, to the best of our knowledge, the most recent lattice calculation of the $D \to \rho$, K^* form factors dates back to 1995 [42]. As significant improvements have recently been made in lattice QCD, a calculation of the $D \to V$ form factors exploiting the current state-of-the-art methods would be very desirable for testing LFU in the charm sector.

In our work, we complement the lattice QCD (LQCD) calculation in Ref. [42] with the results from Ref. [43], using light-cone sum rules (LCSR). The latter calculation is done in the framework of Heavy Quark Effective Field Theory (HQEFT). It should be mentioned that HQEFT, as the name suggests, relies on the assumption of a heavy quark, which in the case of D mesons has to be treated carefully [44]. The definitions and different parametrizations of the form factors are given in Appendix A. The resulting SM predictions for the branching fractions and the corresponding experimental results are summarized in Table 3. For the SM predictions, we use the values for $|V_{cd}|$ and $|V_{cs}|$ in Eqs. (10) and (11), respectively.

4.2.1 Constraints on pseudoscalar coefficients

If we allow for pseudoscalar NP interactions, we obtain the following expression for the differential branching fraction for semileptonic D decays with vector mesons in the final state:

$$\frac{d\mathcal{B}(D \to V\bar{\ell}\nu_\ell)}{dq^2} = \frac{G_F^2 \tau_D |V_{cq}|^2}{24\pi^3 M_D^2} \left\{ \left[\frac{1}{4}\left(1 + \frac{m_\ell^2}{2q^2}\right)\left[(H_{V,+}^V)^2 \right. \right. \right.$$
$$\left. + (H_{V,-}^V)^2 + (H_{V,0}^V)^2\right]$$
$$+ \frac{3}{8}\frac{m_\ell^2}{q^2}(H_{V,t}^V)^2 \right] + \frac{3}{8}|C_P^\ell|^2(H_S^V)^2$$
$$+ \frac{3}{4}\mathcal{R}e(C_P^{\ell*})\frac{m_\ell}{\sqrt{q^2}}H_S^V H_{V,t}^V \right\} \frac{(q^2 - m_\ell^2)^2}{q^2}|\vec{p}_V|, \tag{41}$$

where the terms in the large square brackets represent the SM part. In order to constrain the pseudoscalar NP coefficients C_P^ℓ, we introduce the ratios

$$\mathcal{R}^\mu_{\mu;\rho} \equiv \frac{\mathcal{B}(D^+ \to \mu^+\nu_\mu)}{\mathcal{B}(D^+ \to \rho^0\mu^+\nu_\mu)},$$
$$\mathcal{R}^\mu_{\mu;\overline{K}^*} \equiv \frac{\mathcal{B}(D_s^+ \to \mu^+\nu_\mu)}{\mathcal{B}(D^+ \to \overline{K}^*(892)^0\mu^+\nu_\mu)}. \tag{42}$$

Since each of these observables depends on C_P^μ, they can be used to complement the constraints for this coefficient following from the leptonic D decays. Note that for the $D^+ \to \rho^0\mu^+\nu_\mu$ channel, a factor of 1/2 has to be taken into account due to the wave function of the ρ^0 meson. Using the measured branching fractions in Table 3, we obtain the following experimental values:

$$\mathcal{R}^\mu_{\mu;\rho} = (1.56 \pm 0.27) \times 10^{-1},$$
$$\mathcal{R}^\mu_{\mu;\overline{K}^*} = (1.04 \pm 0.05) \times 10^{-1}. \tag{43}$$

These constraints can be converted correspondingly into allowed ranges for C_P^μ, employing $c \to d$ and $c \to s$ transitions. The results are listed in Table 4, utilizing information on the form factors both from LQCD and from LCSR calculations.

We may use the obtained ranges for C_P^μ to further constrain the allowed regions shown in Figs. 1 and 2. This yields the vertical bands in Figs. 11 and 12. The constraints obtained using LQCD and LCSR form-factor information are indicated by the green and yellow bands, respectively. The dashed-dotted lines in Figs. 11 (right) and 12 (right) indicate the correlations arising from $C_P^e = C_P^\mu$. In both cases, we find no large discrepancies with the SM predictions where the pseudoscalar NP coefficients vanish.

4.2.2 Constraints on vector coefficients

Besides pseudoscalar NP interactions, semileptonic D decays with a vector meson in the final state are also sensitive probes
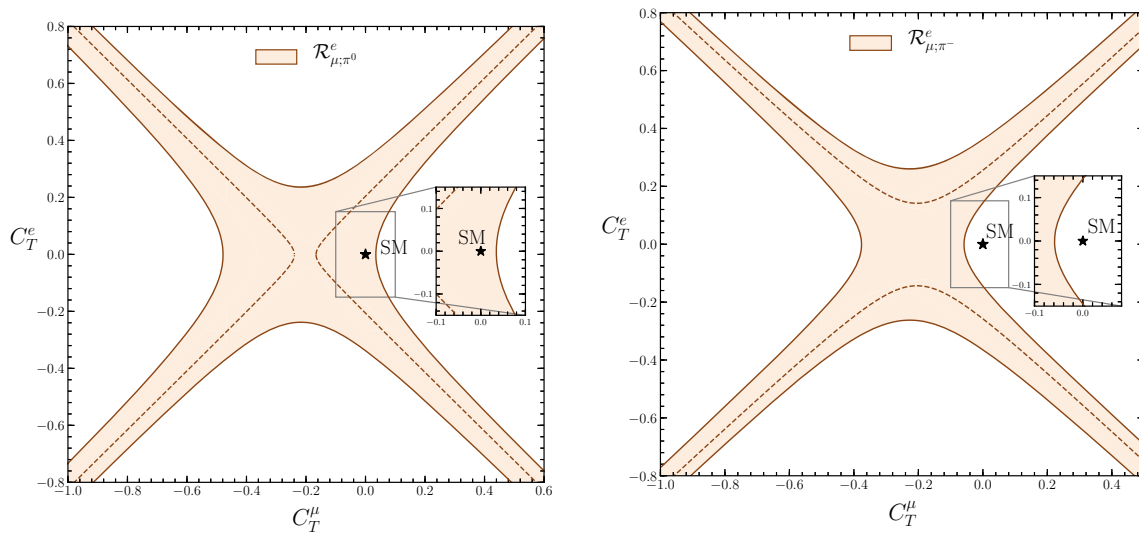
Fig. 9 Allowed regions in the $C_T^\mu - C_T^e$ plane using the ratios $\mathcal{R}_{\mu;\pi^0}^e$ (left) and $\mathcal{R}_{\mu;\pi^-}^e$ (right)
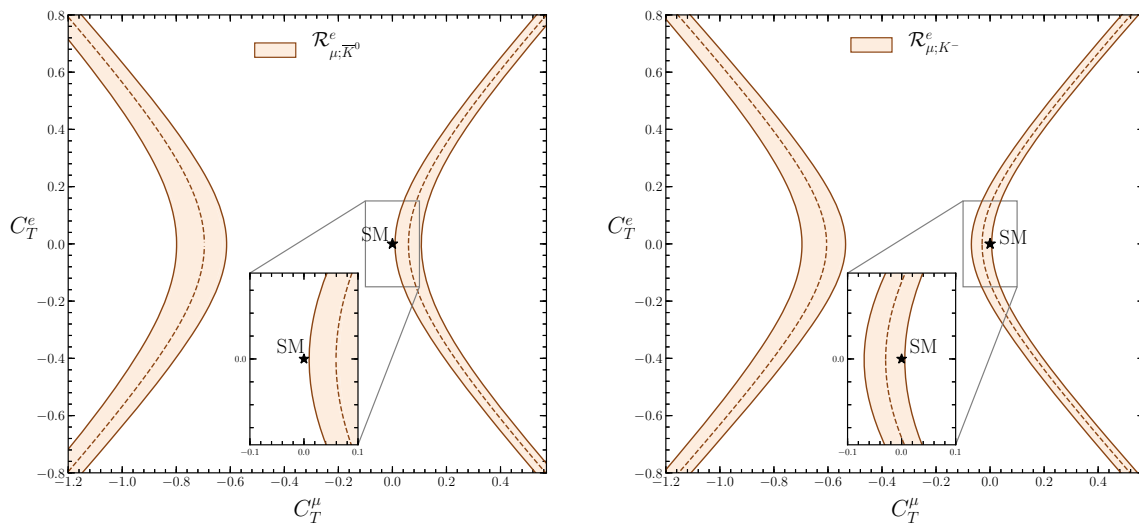

Fig. 10 Allowed regions in the $C_T^\mu - C_T^e$ plane using the ratios $\mathcal{R}_{\mu;\overline{K}^0}^e$ (left) and $\mathcal{R}_{\mu;K^-}^e$ (right)

Table 3 SM predictions for $D \to V\bar{\ell}\nu_\ell$ branching ratios using LQCD and LCSR form-factor information from Refs. [42] and [43], respectively; the experimental values are from Ref. [30]

Decay	LQCD	LCSR	Experiment
$\mathcal{B}(D^+ \to \rho^0 e^+\nu_e)$	$(2.23 \pm 0.70) \times 10^{-3}$	$(2.25 \pm 0.28) \times 10^{-3}$	$(2.18^{+0.17}_{-0.25}) \times 10^{-3}$
$\mathcal{B}(D^+ \to \overline{K}^*(892)^0 e^+\nu_e)$	$(6.26 \pm 1.84) \times 10^{-2}$	$(5.02 \pm 0.56) \times 10^{-2}$	$(5.40 \pm 0.10) \times 10^{-2}$
$\mathcal{B}(D^+ \to \rho^0 \mu^+\nu_\mu)$	$(2.13 \pm 0.64) \times 10^{-3}$	$(2.14 \pm 0.27) \times 10^{-3}$	$(2.4 \pm 0.4) \times 10^{-3}$
$\mathcal{B}(D^+ \to \overline{K}^*(892)^0 \mu^+\nu_\mu)$	$(5.95 \pm 1.67) \times 10^{-2}$	$(4.75 \pm 0.53) \times 10^{-2}$	$(5.27 \pm 0.15) \times 10^{-2}$

of LH and RH vector contributions from physics beyond the SM. The differential branching fraction in the presence of LH vector NP interactions can be written as

$$\frac{d\mathcal{B}(D \to V\bar{\ell}\nu_\ell)}{dq^2} = \frac{d\mathcal{B}(D \to V\bar{\ell}\nu_\ell)}{dq^2}\bigg|_{SM} |1 + C_{V_L}|^2. \quad (44)$$
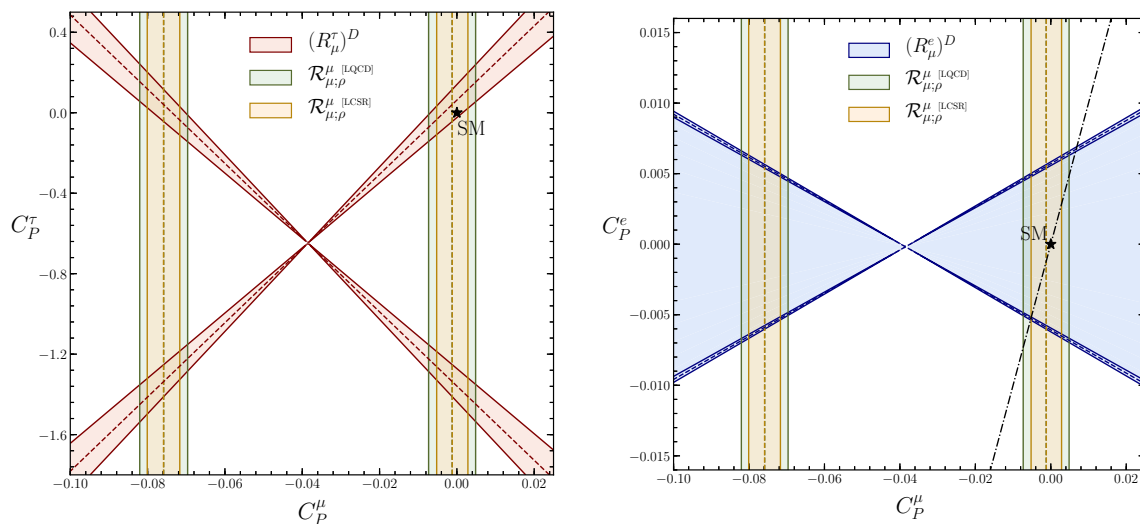
Fig. 11 Allowed regions in the C_P^μ–C_P^τ (left) and C_P^μ–C_P^e (right) planes using the ratios $(R_\mu^\tau)^D$, $\mathcal{R}_{\mu;\rho}^\mu$ and $(R_\mu^e)^D$, $\mathcal{R}_{\mu;\rho}^\mu$, respectively. The dashed-dotted line corresponds to $C_P^e = C_P^\mu$
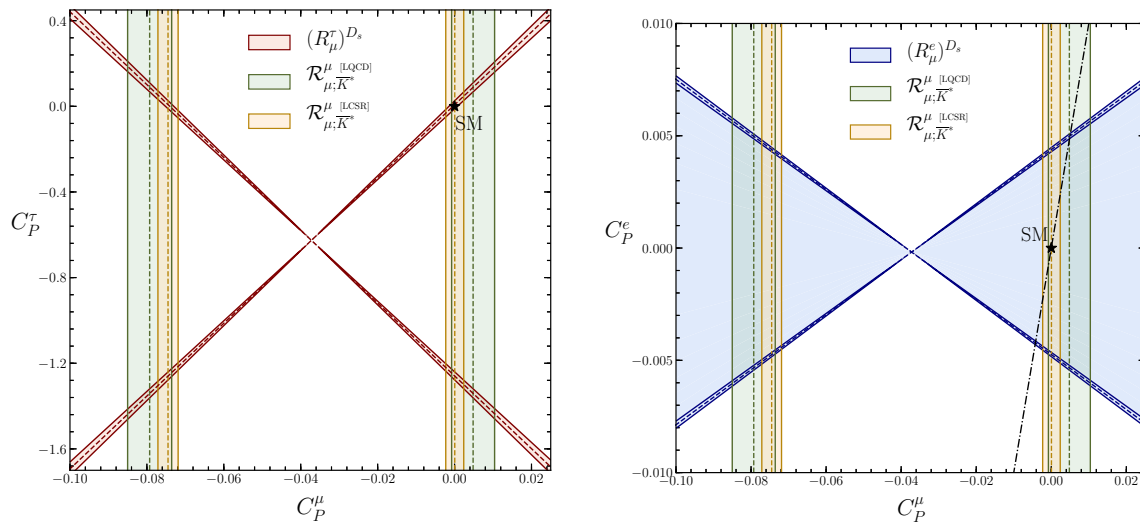

Fig. 12 Allowed regions in the C_P^μ–C_P^τ (left) and C_P^μ–C_P^e (right) planes using the ratios $(R_\mu^\tau)^{D_s}$, $\mathcal{R}_{\mu;\overline{K}^*}^\mu$ and $(R_\mu^e)^{D_s}$, $\mathcal{R}_{\mu;\overline{K}^*}^\mu$, respectively. The dashed-dotted line corresponds to $C_P^e = C_P^\mu$

Table 4 Allowed values for the coefficients $C_P^\mu\big|_{cd}$ and $C_P^\mu\big|_{cs}$, obtained through the ratios $\mathcal{R}_{\mu;\rho}^\mu$ and $\mathcal{R}_{\mu;\overline{K}^*}^\mu$, respectively, using LQCD [42] and LCSR [43] form-factor information

Coefficient	LQCD	LCSR
$C_P^\mu\big|_{cd}$	$(-7.58 \pm 0.62) \times 10^{-2}$	$(-7.59 \pm 0.42) \times 10^{-2}$
	$(-1.23 \pm 6.08) \times 10^{-3}$	$(-1.19 \pm 4.04) \times 10^{-3}$
$C_P^\mu\big|_{cs}$	$(-7.93 \pm 0.57) \times 10^{-2}$	$(-7.45 \pm 0.26) \times 10^{-2}$
	$(4.82 \pm 5.59) \times 10^{-3}$	$(0.05 \pm 2.34) \times 10^{-3}$

In analogy to decays with pseudoscalar mesons in the final states, the ratio between a leptonic and semileptonic decay does not yield further constraints since the additional LH vector contributions cancel. The differential branching fraction in the presence of RH vector NP interactions is slightly different from the pseudoscalar case [25]:

$$\frac{d\mathcal{B}(D \to V\bar{\ell}\nu_\ell)}{dq^2} = \frac{G_F^2 \tau_D |V_{cq}|^2}{24\pi^3 M_D^2} \left\{ \left[\frac{1}{4}\left(1 + \frac{m_\ell^2}{2q^2}\right)\left[(H_{V,+}^V)^2 \right.\right.\right.$$
$$\left. + (H_{V,-}^V)^2 + (H_{V,0}^V)^2 \right] + \frac{3}{8}\frac{m_\ell^2}{q^2}(H_{V,t}^V)^2 \Big](1 + |C_{V_R}^\ell|^2)$$
$$- 2\mathcal{R}e(C_{V_R}^{\ell*})\left[\frac{1}{4}\left(1 + \frac{m_\ell^2}{2q^2}\right)\left[(H_{V,0}^V)^2 + 2H_{V,+}^V H_{V,-}^V\right]\right.$$
$$\left.\left. + \frac{3}{8}\frac{m_\ell^2}{q^2}(H_{V,t}^V)^2\right]\right\}\frac{(q^2 - m_\ell^2)^2}{q^2}|\vec{p}_V|. \tag{45}$$

However, the structure of the formulae does prohibit the extractions of further constraints through the ratio between a leptonic and a semileptonic decay with the same lepton flavour. Therefore, in analogy to Eqs. (34) and (35), we define the following ratios between two semileptonic decays with different flavours of leptons:

$$\mathcal{R}_{\mu;\rho}^e \equiv \frac{\mathcal{B}(D^+ \to \rho^0 e^+ \nu_e)}{\mathcal{B}(D^+ \to \rho^0 \mu^+ \nu_\mu)},$$
$$\mathcal{R}_{\mu;\overline{K}^*}^e \equiv \frac{\mathcal{B}(D^+ \to \overline{K}^*(892)^0 e^+ \nu_e)}{\mathcal{B}(D^+ \to \overline{K}^*(892)^0 \mu^+ \nu_\mu)}. \tag{46}$$

From the measured branching fractions in Table 3, we obtain the following experimental constraints:

$$\mathcal{R}_{\mu;\rho}^e = (9.08 \pm 1.75) \times 10^{-1},$$
$$\mathcal{R}_{\mu;\overline{K}^*}^e = 1.02 \pm 0.03. \tag{47}$$

By comparing Eqs. (33) and (44) with each other, it is clear that the contours in the $C_{V_L}^\mu$–$C_{V_L}^e$ planes will be of the same shape; the expressions differ only up to a scale-factor. As the form-factor information for $D \to P$ decays is significantly more precise than for $D \to V$ decays, and the experimental precision is more or less the same, the constraints coming from $D \to V$ decays do not improve the constraints in Figs. 7 and 8. For RH vector interactions, however, the slightly different structure is worth investigating. For $\mathcal{R}_{\mu;\rho}^e$, this leads to the contour shown in Fig. 13 (left), and for $\mathcal{R}_{\mu;\overline{K}^*}^e$, this leads to the contour shown in Fig. 13 (right). In both plots, the SM prediction is included in the 1σ contours.

4.2.3 Constraints on tensor coefficients

Finally, let us have a closer look at NP tensor contributions, which are the final category of potential NP contributions to semileptonic D decays with a vector meson in the final state. Allowing for such an effect, we obtain the following differential branching ratio:

$$\frac{d\mathcal{B}(D \to V\bar{\ell}\nu_\ell)}{dq^2} = \frac{G_F^2 \tau_D |V_{cq}|^2}{24\pi^3 M_D^2}\left\{\left[\frac{1}{4}\left(1 + \frac{m_\ell^2}{2q^2}\right)\left[(H_{V,+}^V)^2 + (H_{V,-}^V)^2\right.\right.\right.$$
$$\left. + (H_{V,0}^V)^2\right] + \frac{3}{8}\frac{m_\ell^2}{q^2}(H_{V,t}^V)^2\Big] + 2|C_T^\ell|^2\left(1 + \frac{2m_\ell^2}{q^2}\right)\left[(H_{T,+}^V)^2\right.$$
$$\left. + (H_{T,-}^V)^2 + (H_{T,0}^V)^2\right]$$

$$-3\mathcal{R}e(C_T^{\ell*})\frac{m_\ell}{\sqrt{q^2}}(H_{T,0}^V H_{V,0}^V + H_{T,+}^V H_{V,-}^V$$
$$-H_{T,-}^V H_{V,+}^V)\Big\}\frac{(q^2 - m_\ell^2)^2}{q^2}|\vec{p}_V|. \tag{48}$$

However, to the best of our knowledge, there is no explicit lattice calculation of the tensor form factors for $D \to V$ decays available. In Ref. [43], the tensor form factors are related to the vector and scalar form factors A_1, A_2, A_3, V in the framework of HQEFT. A lattice determination of the tensor form factors in $D \to V$ transitions would be very desirable. However, as currently no lattice information is available for these quantities, we will use the HQEFT relations to obtain constraints, albeit for illustrative purpose. The relations for the form factors are given as follows [43]:

$$T_1(q^2) = \frac{M_D^2 - m_V^2 + q^2}{2M_D}\frac{V(q^2)}{M_D + m_V}$$
$$+ \frac{M_D + m_V}{2M_D}A_1(q^2), \tag{49}$$
$$T_2(q^2) = \frac{2}{M_D^2 - m_V^2}\left[\frac{(M_D - y)(M_D + m_V)}{2}A_1(q^2)\right.$$
$$\left. + \frac{M_D(y^2 - m_V^2)}{M_D + m_V}V(q^2)\right], \tag{50}$$
$$T_3(q^2) = -\frac{M_D + m_V}{2M_D}A_1(q^2) + \frac{M_D - m_V}{2M_D}\left[A_2(q^2) - A_3(q^2)\right]$$
$$+ \frac{M_D^2 + 3m_V^2 - q^2}{2M_D(M_D + m_V)}V(q^2). \tag{51}$$

where $y = (M_D^2 + m_V^2 - q^2)/(2M_D)$ is the energy of the vector meson. We use the ratios defined in Eq. (46) and allow for tensor contributions instead of vector contributions. Using the HQEFT relations and the experimental information, we find the allowed regions in the C_T^μ–C_T^e plane shown in Fig. 14. We observe that the SM points fall just within in the 1σ regions in both cases.

5 Determination of $|V_{cd}|$ and $|V_{cs}|$

The determination of $|V_{cd}|$ or $|V_{cs}|$ is done by exploiting data from charged-current interactions involving $c \to d\bar{\ell}\nu_\ell$ or $c \to s\bar{\ell}\nu_\ell$ quark-level transitions, respectively. Usually, these determinations assume just the corresponding SM expressions. However, there may be NP contributions present in these processes, as is the main focus of our analysis. In the case of (semi)-leptonic $D_{(s)}$ decays, their SM expressions could be used to determine $|V_{cd(s)}|$ from the data and non-perturbative information on the hadronic parameters. In Sect. 2.2, we have determined $|V_{cd(s)}|$ independently of $D_{(s)}$ decays, utilizing the Wolfenstein parametrization of the
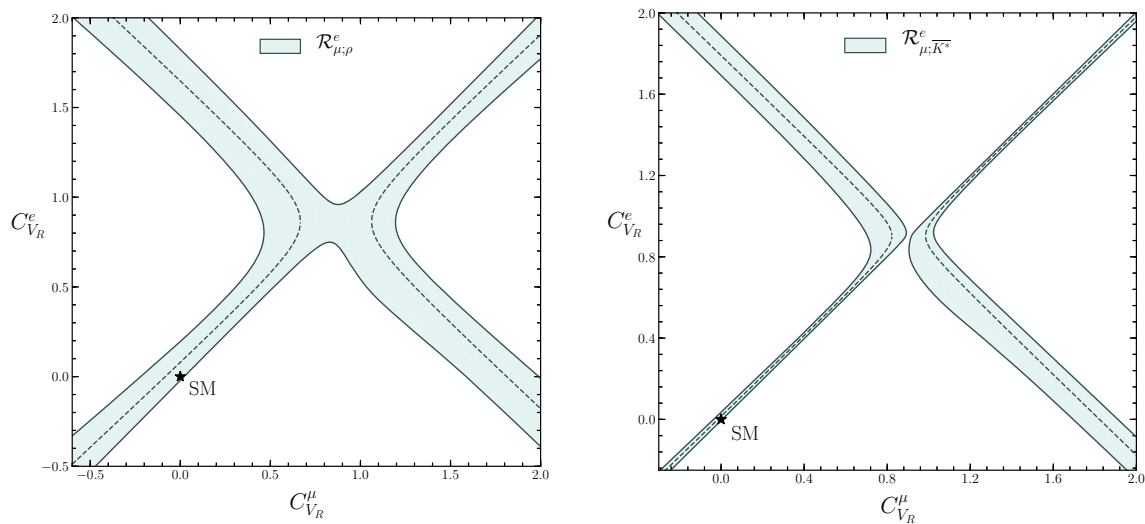
Fig. 13 Allowed regions in the $C_{V_R}^{\mu}$–$C_{V_R}^{e}$ plane using the ratios $\mathcal{R}_{\mu;\rho}^{e}$ (left) and $\mathcal{R}_{\mu;\overline{K}^*}^{e}$ (right)
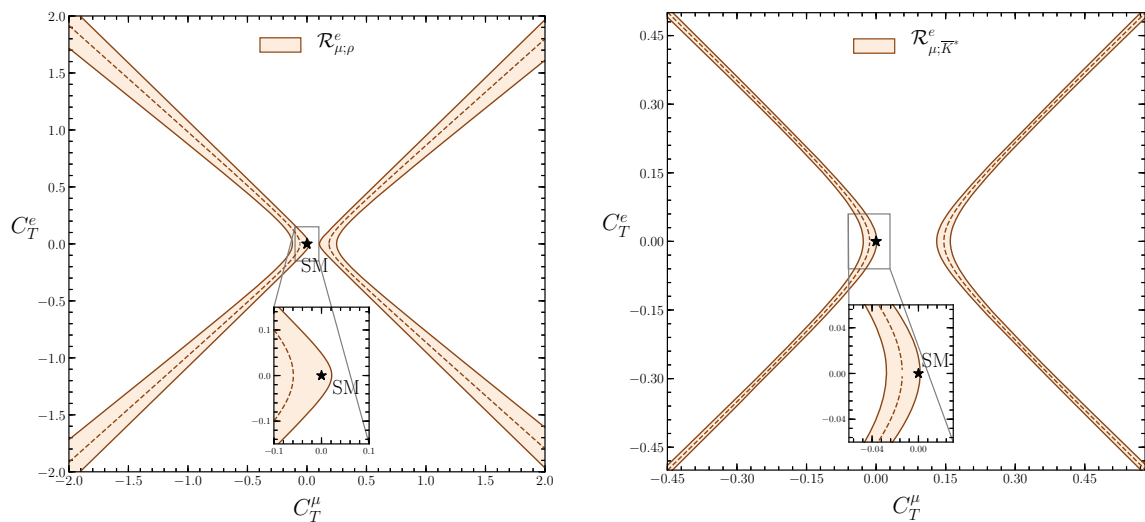

Fig. 14 Allowed regions in the C_T^{μ}–C_T^{e} plane using the ratios $\mathcal{R}_{\mu;\rho}^{\mu}$ (left) and $\mathcal{R}_{\mu;\overline{K}^*}^{\mu}$ (right)

CKM matrix. Here, we have assumed the SM in the corresponding kaon and B decay processes.

Physics beyond the SM may also affect the values of the CKM matrix elements. Consequently, we have probed NP through observables that do not involve such parameters. Combining the theoretical expressions for these observables with experimental information on the branching fractions allows us to constrain NP coefficients, independently of the CKM matrix elements. Finally, having these constraints available, we may use them to extract $|V_{cd(s)}|$ from $D_{(s)}$ decays, even in the presence of possible NP effects in the corresponding transition amplitudes.

5.1 The strategy

In our analysis, we follow a strategy first proposed for B decays in Ref. [22]. It has not yet been applied to the charm sector. Using the NP constraints obtained from the observables $\mathcal{R}_{\mu;\rho}^{\mu}$ and $\mathcal{R}_{\mu;\overline{K}^*}^{\mu}$, we will finally also determine $|V_{cd}|$ or $|V_{cs}|$ in the presence of pseudoscalar NP contributions. To distinguish the coefficients corresponding either to a $c \rightarrow d$ transition or a $c \rightarrow s$ transition, we denote the latter with $\tilde{C}_P^{\mu}$. There are three steps in this approach, after which we obtain the CKM matrix elements:

- We start with the expressions for $\mathcal{R}^\mu_{\mu;\rho}$ and $\mathcal{R}^\mu_{\mu;\overline{K}^*}$ in Eq. (42), which depend only on one coefficient, either C_P^μ or $\tilde{C}_P^\mu$. Consequently, we can solve for C_P^μ or $\tilde{C}_P^\mu$.
- This results in the functions $C_P^\mu(\mathcal{R}^\mu_{\mu;\rho})$ and $\tilde{C}_P^\mu(\mathcal{R}^\mu_{\mu;\overline{K}^*})$. For both functions, there are two independent solutions for the coefficients, corresponding to the two bands shown in Figs. 11 and 12.
- We then evaluate any of the individual branching fractions for each of these ratios and solve for the corresponding CKM matrix element. Comparing the resulting expression to individual measurements of the branching fractions allows us to obtain the value of $|V_{cd}|$ or $|V_{cs}|$.

5.2 $|V_{cd}|$ and $|V_{cs}|$

We apply the described strategy to leptonic and semileptonic $D_{(s)}$ decays to determine the CKM matrix elements $|V_{cd}|$ and $|V_{cs}|$. To this end, we recall the following ratios:

$$
\begin{aligned}
\mathcal{R}^\mu_{\mu;\rho} &= \frac{\mathcal{B}(D^+ \to \mu^+\nu_\mu)}{\mathcal{B}(D^+ \to \rho^0\mu^+\nu_\mu)}, \\
\mathcal{R}^\mu_{\mu;\overline{K}^*} &= \frac{\mathcal{B}(D_s^+ \to \mu^+\nu_\mu)}{\mathcal{B}(D^+ \to \overline{K}^*(892)^0\mu^+\nu_\mu)},
\end{aligned}
\tag{52}
$$

which were given in Sect. 4.2.2, along with the theoretical expressions for the branching fractions including pseudoscalar NP contributions. Using these expressions, we write the ratios as follows:

$$
\mathcal{R}^\ell_{\ell;V} = \frac{\tilde{\alpha}^\ell \left|1 + \beta^\ell C_P^\ell\right|^2}{\mathcal{I}_1 + \mathcal{I}_2|C_P^\ell|^2 + \mathcal{I}_3\mathrm{Re}(C_P^{\ell*})},
\tag{53}
$$

where $V = \rho, \overline{K}^*$ and $\tilde{\alpha}^\ell = \alpha^\ell f_D^2$. To keep the notation clear, the subscript s is omitted; in the case $\mathcal{R}^\mu_{\mu;\overline{K}^*}$ the notation $D \to D_s$ and $C_P^\ell \to \tilde{C}_P^\ell$ is implied. The integrals $\mathcal{I}_1$, $\mathcal{I}_2$, $\mathcal{I}_3$ take the forms

$$
\begin{aligned}
\mathcal{I}_1 &= I_0 \int_{m_\ell^2}^{(M_D-m_V)^2} dq^2 \left[\frac{1}{4}\left(1 + \frac{m_\ell^2}{2q^2}\right)\left[(H_V^+)^2 + (H_V^-)^2\right.\right. \\
&\quad \left.\left. + (H_V^0)^2\right] + \frac{3}{8}\frac{m_\ell^2}{q^2}(H_V^t)^2\right]\frac{(q^2-m_\ell^2)^2}{q^2}|\vec{p}_V|, \\
\mathcal{I}_2 &= I_0 \int_{m_\ell^2}^{(M_D-m_V)^2} dq^2 \frac{3}{8}(H_P^0)^2\frac{(q^2-m_\ell^2)^2}{q^2}|\vec{p}_V|, \\
\mathcal{I}_3 &= I_0 \int_{m_\ell^2}^{(M_D-m_V)^2} dq^2 \frac{3}{4}\frac{m_\ell}{\sqrt{q^2}}H_P^0 H_V^t\frac{(q^2-m_\ell^2)^2}{q^2}|\vec{p}_V|,
\end{aligned}
\tag{54}
$$

where $I_0 = 1/(3\pi^2 M_D^2)$. Note that for $\mathcal{R}^\mu_{\mu;\overline{K}^*}$, an additional factor of τ_{D_s}/τ_D should be included, as the decaying D mesons in the leptonic and semileptonic decays are different. We assume the coefficients to be real and

solve for $C_{V_R}^\mu$, $\tilde{C}_{V_R}^\mu$. The resulting expressions are the functions $C_P^\mu(\mathcal{R}^\mu_{\mu;\rho})$ and $\tilde{C}_P^\mu(\mathcal{R}^\mu_{\mu;\overline{K}^*})$. Subsequently, we insert $C_P^\mu(\mathcal{R}^\mu_{\mu;\rho})$ and $\tilde{C}_P^\mu(\mathcal{R}^\mu_{\mu;\overline{K}^*})$ in the expressions for the (semi)-leptonic branching fractions and solve for the corresponding CKM element. For the leptonic branching fractions, this yields:

$$
|V_{cq}| = \left(\frac{8\pi\mathcal{B}(D_{(s)}^+ \to \mu^+\nu_\mu)}{G_F^2\tau_{D_{(s)}}\alpha^\mu\left|1 + \beta^\mu C_P^\mu(\mathcal{R}^\mu_{\mu;V})\right|^2}\right)^{1/2}.
\tag{55}
$$

As there are two solutions for C_P^μ and $\tilde{C}_P^\mu$, corresponding to the either of the two vertical bands in Figs. 11 and 12, we obtain two independent solutions for the each of the CKM matrix elements. Using the form factors calculated in LQCD [42], these results are equivalent at the current level of precision. In both cases, we obtain

$$
|V_{cd}| = 0.227 \pm 0.037,
\tag{56}
$$
$$
|V_{cs}| = 0.880 \pm 0.115.
\tag{57}
$$

Using the LCSR [43] form-factor information, we obtain the following results:

$$
|V_{cd}| = 0.227 \pm 0.027 \vee |V_{cd}| = 0.227 \pm 0.025,
\tag{58}
$$

$$
|V_{cs}| = 0.992 \pm 0.080 \vee |V_{cs}| = 0.993 \pm 0.066.
\tag{59}
$$

In Table 5, we list the values for the CKM elements obtained in Sect. 2.2, denoted as V_{UT}, the values determined in the presence of pseudoscalar NP, denoted as $V_{\mathrm{LQCD}}^{\mathrm{NP}}$ and $V_{\mathrm{LCSR}}^{\mathrm{NP}}$, and the PDG values, denoted as V_{PDG}. For both $|V_{cd}|$ and $|V_{cs}|$, the obtained values allowing for pseudoscalar NP agree with the SM and PDG values at the 1σ level. This was to be expected, as we did not find large deviations from the SM when investigating NP contributions. Although our determined values have considerably larger uncertainties, the aim here is to show how to properly account for NP in the determination of CKM elements. Interestingly, there are discrepancies between our UT value and the PDG value assuming the SM of 1.5σ and 1.4σ for $|V_{cd}|$ and $|V_{cs}|$, respectively.

6 Predictions for branching fractions

Now that we have constraints on the pseudoscalar NP coefficients and determinations of the CKM elements at our disposal, we may combine them to make predictions for the following leptonic branching fractions that have yet to be measured:

$$
\mathcal{B}(D^+ \to e^+\nu_e), \qquad \mathcal{B}(D_s^+ \to e^+\nu_e).
\tag{60}
$$

Table 5 The CKM matrix elements $|V_{cd}|$ and $|V_{cs}|$ obtained in the present analysis and their PDG values [30]. $\Delta_{|V_{cd}|}$ and $\Delta_{|V_{cs}|}$ denote the differences between the indicated values in standard deviations

	V_{UT}	$V_{\text{LQCD}}^{\text{NP}}$	$V_{\text{LCSR}}^{\text{NP}}$	V_{PDG}
$|V_{cd}|$	0.2242 ± 0.0005	0.227 ± 0.037	0.227 ± 0.027	0.218 ± 0.004
		0.227 ± 0.037	0.227 ± 0.025	
$|V_{cs}|$	0.9736 ± 0.0001	0.880 ± 0.115	0.992 ± 0.080	0.997 ± 0.017
		0.880 ± 0.115	0.993 ± 0.066	

	$V_{\text{LQCD}}^{\text{NP}} - V_{\text{UT}}$	$V_{\text{LCSR}}^{\text{NP}} - V_{\text{UT}}$	$V_{\text{LQCD}}^{\text{NP}} - V_{\text{PDG}}$	$V_{\text{LCSR}}^{\text{NP}} - V_{\text{PDG}}$
$\Delta_{|V_{cd}|}$	0.07	0.09	0.24	0.31
	0.08	0.10	0.24	0.34
$\Delta_{|V_{cs}|}$	0.82	0.23	1.01	0.06
	0.81	0.29	1.01	0.07
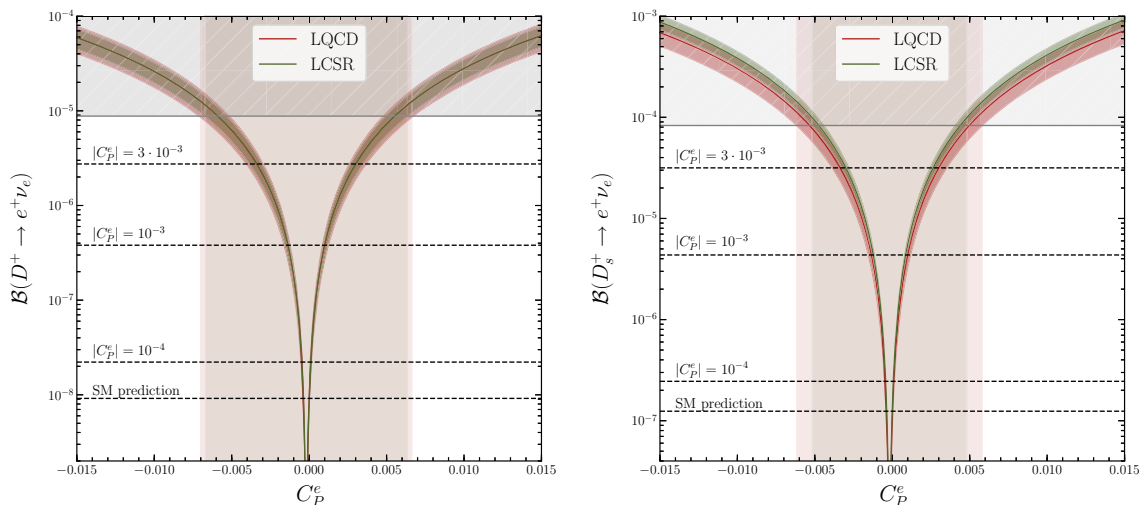
Fig. 15 $\mathcal{B}(D_{(s)}^+ \to e^+ \nu_e)$ as functions of C_P^e. The grey regions indicate experimentally excluded regions, while the red and green ones show the allowed values for C_P^e

In the SM, these decays are strongly helicity suppressed, as indicated by the smallness of the corresponding SM predictions in Table 1. However, this suppression may be lifted by new pseudoscalar interactions. This is shown in Fig. 15. Here, the branching fractions $\mathcal{B}(D^+ \to e^+ \nu_e)$ and $\mathcal{B}(D_s^+ \to e^+ \nu_e)$ are plotted as a function of the coefficient C_P^e. The labels "LQCD" and "LCSR" refer to the form-factor information used to determine the relevant CKM elements in the presence of pseudoscalar NP, given in Eqs. (56–59). The grey regions indicate the experimental upper bounds on the branching fractions. In order to illustrate the sensitivity of the branching fractions to the absolute value of C_P^e, the SM prediction and three predictions for different values of $|C_P^e|$ are shown in each plot. We see that even a small value for $|C_P^e|$ has a potentially large effect on the branching fraction, which is a direct consequence of the pseudoscalar NP contributions lifting the helicity suppression in these decays.

At the same time, the obtained constraints on the NP coefficients allow us to predict the branching fractions discussed here in the context of different scenarios related to LFU violation. Let us consider the following scenarios:

- $C_P^e = C_P^\mu$. This correlation is indicated by the dashed-dotted lines in Figs. 11 (right) and 12 (right).
- $C_P^e = (m_e/m_\mu)C_P^\mu$. This correlation arises, for instance, in the context of a type II Two-Higgs-Doublet model.
- $C_P^e \gg C_P^\mu$. We probe the impact of $C_P^e = 10 C_P^\mu$ on the relevant branching fractions.
- $C_P^e \ll C_P^\mu$. Similar to the previous scenario, but focusing on the effect of setting $C_P^e = 10^{-1} C_P^\mu$ for the corresponding branching fractions.

We use the obtained constraints on C_P^μ, given in Table 4, and relate them to C_P^e in each scenario accordingly. Subsequently, we use the corresponding values for the CKM
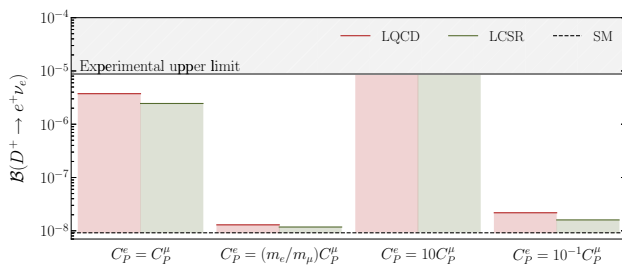
Fig. 16 Predictions of $\mathcal{B}(D^+ \to e^+ \nu_e)$ for the scenarios discussed in the text. The red and green bands indicate the LQCD and LCSR form-factor information used. The grey line is the experimental upper limit, while the dashed line is the SM prediction
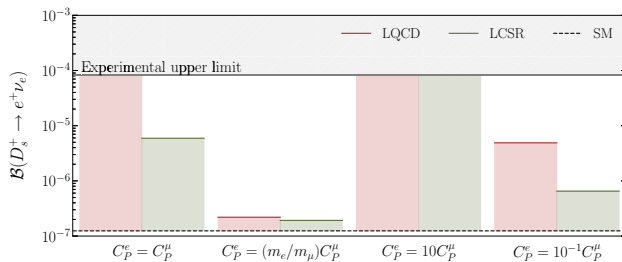

Fig. 17 Predictions of $\mathcal{B}(D_s^+ \to e^+ \nu_e)$ for the scenarios discussed in the text. The red and green bands indicate the LQCD and LCSR form-factor information used. The grey line is the experimental upper limit, while the dashed line is the SM prediction

elements, given in Table 5, and apply the results to Eq. (15) to obtain a theoretical prediction for the branching fractions $\mathcal{B}(D^+ \to e^+ \nu_e)$ and $\mathcal{B}(D_s^+ \to e^+ \nu_e)$ in each of the scenarios. In Figs. 16 and 17, we compare our predictions to the corresponding SM predictions, where $C_P^e = C_P^\mu = 0$. For the SM prediction, the $|V_{cd(s)}|$ values obtained from unitarity were used. The determination of the relevant CKM elements using LQCD or LCSR form-factor information is indicated by the red and green colours of the bars, respectively. Furthermore, the grey regions indicate the values that are currently already excluded by experiment.

It is interesting to see that in the case $C_P^e = C_P^\mu$ in Fig. 16, our predictions for $\mathcal{B}(D^+ \to e^+ \nu_e)$ are very close to the experimental upper limit. For $\mathcal{B}(D_s^+ \to e^+ \nu_e)$ illustrated in Fig. 17, our predictions using either LQCD or LCSR based form-factor calculations differ substantially, underlining the importance of precise lattice information on the semileptonic form factors. An observation of spectacularly enhanced $D_{(s)}^+ \to e^+ \nu_e$ modes close to the current experimental limits would be an unambiguous signal of physics beyond the SM.

7 Conclusions

We have presented a comprehensive analysis of (semi)-leptonic $D_{(s)}$-meson decays to constrain possible effects of physics from beyond the SM arising from new (pseudo)-

scalar, vector and tensor operators, allowing also for violations of LFU. The central role is played by various ratios of decay rates that are independent of the CKM matrix elements $|V_{cd}|$ and $|V_{cs}|$. In the case of leptonic decays, the decay constants cancel there and in the case of combinations of leptonic and semileptonic decays, ratios of non-perturbative hadronic parameters arise that are usually more precise than the individual parameters.

We obtain a picture in agreement with the SM, including a few deviations at the 1σ level. Following our strategy, we may also determine $|V_{cd}|$ and $|V_{cs}|$ from the (semi)-leptonic decays in the presence of NP contributions. The corresponding results are fully consistent with values arising from the unitarity of the CKM matrix and the Wolfenstein parameterization that do not involve any experimental input from the charm system. We have identified various form factors with interesting potential for future improvement through lattice QCD calculations.

The leptonic $D_{(s)}^+ \to e^+ \nu_e$ decays are hugely helicity suppressed in the SM. However, this suppression may be lifted through new pseudoscalar interactions. Using the constraints following from the interplay between leptonic $D_{(s)}$ decays with muon or tau leptons in the final state and $D \to V \bar{\ell} \nu_\ell$ decays, we illustrate that the branching ratio for $D_{(s)}^+ \to e^+ \nu_e$ may be hugely enhanced and could enter the regime close to the current experimental upper bounds. A future observation of these modes would be an unambiguous signal of NP effects.

We look forward to obtaining stronger constraints on possible violations of LFU in the charged-current interactions in $D_{(s)}$ decays in the high-precision era of quark-flavour physics which is ahead of us.

A Form factors

A.1 $D \to P$

The form factors for $D \to P$ decays in the helicity basis are defined as follows [25]:

$$H_{V,s}^P = \frac{M_{D_{(s)}}^2 - m_P^2}{\sqrt{q^2}} f_0(q^2), \tag{61a}$$

$$H_{V,0}^P = \sqrt{\frac{\lambda_P(q^2)}{q^2}} f_+(q^2), \tag{61b}$$

$$H_{V,\pm}^P = 0, \tag{61c}$$

$$H_{S,s}^P = \frac{M_{D_{(s)}}^2 - m_P^2}{m_c - m_q} f_0(q^2), \tag{61d}$$

$$H_{P,s}^P = 0, \tag{61e}$$

$$H_T^P = -\frac{\sqrt{\lambda_P(q^2)}}{M_{D_{(s)}} + m_P} f_T(q^2), \tag{61f}$$

where $\lambda_P(q^2) = [(M_{D_{(s)}} - m_P)^2 - q^2][(M_{D_{(s)}} + m_P)^2 - q^2]$. For our calculations, we adopt the z-series parametrization from Ref. [38]. For the $D \to \pi$ case, the scalar and vector form factors are given by

$$f_+^{D \to \pi}(q^2) = \frac{f^{D \to \pi}(0) + c_+^{D \to \pi}(z - z_0)(1 + \frac{1}{2}(z + z_0))}{1 - P_V q^2}, \tag{62}$$

$$f_0^{D \to \pi}(q^2) = \frac{f^{D \to \pi}(0) + c_0^{D \to \pi}(z - z_0)(1 + \frac{1}{2}(z + z_0))}{1 - P_S q^2}, \tag{63}$$

where $z_0 = z(0, t_0^\pi)$. In the case of $D \to K$ transitions, the scalar and vector form factors are parametrized as

$$f_+^{D \to K}(q^2) = \frac{f^{D \to K}(0) + c_+^{D \to K}(z - z_0)(1 + \frac{1}{2}(z + z_0))}{1 - q^2/M_{D_s^*}^2}, \tag{64}$$

$$f_0^{D \to K}(q^2) = f^{D \to K}(0) + c_0^{D \to K}(z - z_0)\left(1 + \frac{1}{2}(z + z_0)\right), \tag{65}$$

where $z_0 = z(0, t_0^K)$. The fit parameters are listed in Table 6.

Table 6 Fit parameters for f_0, f_+ in the z-series expansion [38]

Decay	$f(0)$	c_+	P_V (GeV)$^{-2}$	c_0	P_S (GeV)$^{-2}$
$D \to \pi$	0.6117 (354)	-1.985 (347)	0.1314 (127)	-1.188 (256)	0.0342 (122)
$D \to K$	0.7647 (308)	-0.066 (333)	–	-2.084 (283)	–

Table 7 Fit parameters for f_T in the z-series expansion [39]

Decay	$f_T(0)$	c_T	P_T (GeV)$^{-2}$
$D \to \pi$	0.5063 (786)	-1.10 (1.03)	0.1461 (681)
$D \to K$	0.6871 (542)	-2.86 (1.46)	0.0854 (671)

Table 8 LQCD fit parameters for the $D \to \rho$ and $D \to K^*$ form factors, taken from Ref. [42]

Decay	Form factor	$F(0)$	$m_{J^P} [a^{-1}]$
$D \to \rho$	A_0	$0.70_{-0.12}^{+0.05}$	$m_{0^-}^{c\bar{d}} = 0.60_{-0.05}^{+0.07}$
	A_1	$0.63_{-0.09}^{+0.06}$	$m_{1^+}^{c\bar{d}} = 1.1_{-0.2}^{+0.3}$
	A_2	$0.51_{-0.15}^{+0.10}$	$m_{1^+}^{c\bar{d}} = 0.44_{-0.05}^{+0.09}$
	V	$0.95_{-0.14}^{+0.29}$	$m_{1^-}^{c\bar{d}} = 0.91_{-0.18}^{+0.36}$
$D \to K^*$	A_0	$0.75_{-0.11}^{+0.05}$	$m_{0^-}^{c\bar{s}} = 0.59_{-0.05}^{+0.06}$
	A_1	$0.70_{-0.10}^{+0.07}$	$m_{1^+}^{c\bar{s}} = 1.1_{-0.2}^{+0.3}$
	A_2	$0.66_{-0.15}^{+0.10}$	$m_{1^+}^{c\bar{s}} = 0.46_{-0.07}^{+0.16}$
	V	$1.01_{-0.13}^{+0.30}$	$m_{1^-}^{c\bar{s}} = 0.85_{-0.15}^{+0.24}$

For the tensor form factor, we use the lattice calculation of Ref. [39]. Here, f_T is parametrized in the following way:

$$f_T^{D \to \pi}(q^2) = \frac{f_T^{D \to \pi}(0) + c_T^{D \to \pi}(z - z_0)(1 + \frac{1}{2}(z + z_0))}{1 - P_T^{D \to \pi} q^2}, \tag{66}$$

$$f_T^{D \to K}(q^2) = \frac{f_T^{D \to K}(0) + c_T^{D \to K}(z - z_0)(1 + \frac{1}{2}(z + z_0))}{1 - P_T^{D \to K} q^2}. \tag{67}$$

The fit parameters are given in Table 7.

A.2 $D \to V$

The non-zero form factors for $D \to V$ decays in the helicity basis are defined as follows [25]:

$$H_{V,\pm}^V = (M_D + m_V) A_1(q^2) \mp \frac{\sqrt{\lambda_V(q^2)}}{M_D + m_V} V(q^2), \tag{68a}$$

$$H_{V,0}^V = \frac{M_D + m_V}{2 M_V \sqrt{q^2}} \left[-(M_D^2 - M_V^2 - q^2) A_1(q^2) + \frac{\lambda_V(q^2)}{(M_D + m_V)^2} A_2(q^2) \right], \tag{68b}$$

Table 9 LCSR fit parameters for the $D \to \rho$ and $D \to K^*$ form factors, taken from Ref. [43]

Decay	Form Factor	$F(0)$	a_F	b_F
$D \to \rho$	A_1	$0.590^{+0.031}_{-0.029}$	$0.44^{-0.04}_{+0.05}$	$0.20^{-0.03}_{+0.10}$
	A_2	$0.528^{+0.036}_{-0.031}$	$0.91^{+0.07}_{-0.13}$	$-1.01^{+0.22}_{-0.41}$
	A_3	$-0.528^{+0.031}_{-0.026}$	$0.91^{-0.13}_{+0.07}$	$-1.01^{-0.41}_{+0.22}$
	V	$0.735^{+0.032}_{-0.025}$	$0.48^{-0.11}_{+0.21}$	$2.25^{-0.21}_{+0.61}$
$D \to K^*$	A_1	$0.601^{+0.030}_{-0.029}$	$0.51^{-0.02}_{+0.02}$	$0.04^{+0.01}_{-0.01}$
	A_2	$0.541^{+0.038}_{-0.033}$	$0.91^{+0.05}_{-0.10}$	$-0.68^{+0.12}_{-0.21}$
	A_3	$-0.541^{+0.033}_{-0.038}$	$0.91^{-0.10}_{+0.05}$	$-0.68^{-0.21}_{+0.12}$
	V	$0.796^{+0.032}_{-0.027}$	$0.60^{-0.07}_{+0.13}$	$1.53^{-0.13}_{+0.30}$

$$H^V_{V,t} = \sqrt{\frac{\lambda_V(q^2)}{q^2}} A_0(q^2), \tag{68c}$$

$$H^V_P = -\frac{\sqrt{\lambda_V(q^2)}}{m_c + m_q} A_0(q^2), \tag{68d}$$

$$H^V_{T,\pm} = \frac{1}{\sqrt{q^2}}\Big[\pm (M_D^2 - m_V^2) T_2(q^2) + \sqrt{\lambda_V(q^2)} T_1(q^2) \Big], \tag{68e}$$

$$H^V_{T,0} = \frac{1}{2m_V}\Big[-(M_D^2 + 3m_V^2 - q^2) T_2(q^2) + \frac{\lambda_V(q^2)}{M_D^2 - m_V^2} T_3(q^2) \Big], \tag{68f}$$

where $\lambda_V(q^2) = [(M_D - m_V)^2 - q^2][(M_D + m_V)^2 - q^2]$. We use the lattice determination of the $D \to \rho$ and $D \to K^*$ semileptonic form factors from Ref. [42]. The q^2 dependence is obtained through a single-pole parametrization:

$$V(q^2) = \frac{V(0)}{1 - q^2/m_{1^-}^2}, \qquad A_0(q^2) = \frac{A_0(0)}{1 - q^2/m_{0^-}^2},$$
$$A_i(q^2) = \frac{A_i(0)}{1 - q^2/m_{1^+}^2}, \tag{69}$$

where $i = 1, 2, 3$ and m_{J^P} denotes the mass of the meson with spin J and parity P corresponding to the relevant quark transition, i.e., $c\bar{d}$ for $D \to \rho$ and $c\bar{s}$ for $D \to K^*$. The values for the parameters are given in Table 8. The masses are listed in units of the inverse lattice spacing, which is given by $a^{-1} = (2.73 \pm 0.05)\,\text{GeV}$. The form factor A_3 is related to the form factors A_1 and A_2 in the following way:

$$A_3(q^2) = \frac{M_D + m_V}{2m_V} A_1(q^2) - \frac{M_D - m_V}{2m_V} A_2(q^2). \tag{70}$$

We complement the lattice calculation with the LCSR calculation of Ref. [43]. This work dates back to 2006, but there exists a more recent determination of the $D \to \rho$ form factors [45]. In this analysis, the massless lepton limit is taken, neglecting the form factor A_0. In our study, we investigate the difference between different lepton flavours, therefore requiring information on A_0. We therefore utilize the form-factor

information of Ref. [43], where the following double-pole parametrization was adopted:

$$F^i(q^2) = \frac{F^i(0)}{1 - a_{F^i} q^2/M_D^2 + b_{F^i}(q^2/M_{D_{(s)}}^2)^2}, \tag{71}$$

with F^i denoting any of the form factors A_1, A_2, A_3 or V. Here, a different convention is used: instead of the set $\{A_0, A_1, A_2\}$, the hadronic matrix elements are parametrized by the set $\{A_1, A_2, A_3\}$. The relation between the different conventions is given by [46]:

$$A_0(q^2) = \frac{1}{2m_V}\Big[(M_D + m_V) A_1(q^2) \\ - (M_D - m_V) A_2(q^2) - \frac{q^2}{M_D + m_V} A_3(q^2) \Big]. \tag{72}$$

The results from LCSR for the fit parameters for $D \to \rho$ and $D \to K^*$ transitions are listed in Table 9.

References

1. A.J. Buras, D. Buttazzo, J. Girrbach-Noe, R. Knegjens, Can we reach the Zeptouniverse with rare K and $B_{s,d}$ decays? JHEP **11**, 121 (2014). arXiv:1408.0728 [hep-ph]
2. Y. Li, C.-D. Lü, Recent anomalies in B physics. Sci. Bull. **63**, 267–269 (2018). arXiv:1808.02990 [hep-ph]
3. S. Bifani, S. Descotes-Genon, A. Romero Vidal, M.H. Schune, Review of lepton universality tests in B decays. J. Phys. **G46**(2), 023001 (2019). arXiv:1809.06229 [hep-ex]
4. Y.S. Amhis et al. (Heavy Flavor Averaging Group), Averages of b-hadron, c-hadron, and τ-lepton properties as of 2018 (2019). arXiv:1909.12524 [hep-ex]
5. R. Aaij et al. (LHCb Collaboration), Search for lepton-universality violation in $B^+ \to K^+\ell^+\ell^-$ decays. Phys. Rev. Lett. **122**(19), 191801 (2019). arXiv:1903.09252 [hep-ex]
6. R. Aaij et al. (LHCb Collaboration), Test of lepton universality with $B^0 \to K^{*0}\ell^+\ell^-$ decays. JHEP **08**, 055 (2017). arXiv:1705.05802 [hep-ex]
7. D. Bečirević, O. Sumensari, A leptoquark model to accommodate $R_K^{\text{exp}} < R_K^{\text{SM}}$ and $R_{K^*}^{\text{exp}} < R_{K^*}^{\text{SM}}$. JHEP **08**, 104 (2017). arXiv:1704.05835 [hep-ph]

8. L. Calibbi, A. Crivellin, T. Li, Model of vector leptoquarks in view of the *B*-physics anomalies. Phys. Rev. D **98**(11), 115002 (2018). arXiv:1709.00692 [hep-ph]

9. M. Blanke, A. Crivellin, *B* meson anomalies in a Pati–Salam model within the Randall–Sundrum background. Phys. Rev. Lett. **121**(1), 011801 (2018)

10. A. Crivellin, C. Greub, D. Müller, F. Saturnino, Importance of loop effects in explaining the accumulated evidence for new physics in B decays with a vector leptoquark. Phys. Rev. Lett. **122**(1), 011805 (2019). arXiv:1807.02068 [hep-ph]

11. C. Cornella, J. Fuentes-Martin, G. Isidori, Revisiting the vector leptoquark explanation of the B-physics anomalies. JHEP **07**, 168 (2019). arXiv:1903.11517 [hep-ph]

12. O. Popov, M.A. Schmidt, G. White, R_2 as a single leptoquark solution to $R_{D^{(*)}}$ and $R_{K^{(*)}}$. Phys. Rev. D **100**(3), 035028 (2019). arXiv:1905.06339 [hep-ph]

13. L. Bian, H.M. Lee, C.B. Park, *B*-meson anomalies and Higgs physics in flavored $U(1)'$ model. Eur. Phys. J. C **78**(4), 306 (2018). arXiv:1711.08930 [hep-ph]

14. B.C. Allanach, T. Corbett, M.J. Dolan, T. You, Hadron collider sensitivity to fat flavourful Z's for $R_{K^{(*)}}$. JHEP **03**, 137 (2019). arXiv:1810.02166 [hep-ph]

15. L. Calibbi, A. Crivellin, F. Kirk, C.A. Manzari, L. Vernazza, Z' models with less-minimal flavour violation (2019). arXiv:1910.00014 [hep-ph]

16. C. Niehoff, P. Stangl, D.M. Straub, Violation of lepton flavour universality in composite Higgs models. Phys. Lett. B **747**, 182–186 (2015). arXiv:1503.03865 [hep-ph]

17. S. Iguro, K. Tobe, $R(D^{(*)})$ in a general two Higgs doublet model. Nucl. Phys. B **925**, 560–606 (2017). arXiv:1708.06176 [hep-ph]

18. A. Crivellin, D. Müller, C. Wiegand, $b \to s\ell^+\ell^-$ transitions in two-Higgs-doublet models. JHEP **06**, 119 (2019). arXiv:1903.10440 [hep-ph]

19. R. Bause, M. Golz, G. Hiller, A. Tayduganov, The new physics reach of null tests with $D \to \pi\ell\ell$ and $D_s \to K\ell\ell$ decays. arXiv:1909.11108 [hep-ph]

20. A. Crivellin, G. D'Ambrosio, M. Hoferichter, L.C. Tunstall, Violation of lepton flavor and lepton flavor universality in rare kaon decays. Phys. Rev. D **93**(7), 074038 (2016). arXiv:1601.00970 [hep-ph]

21. S. Fajfer, I. Nisandzic, U. Rojec, Discerning new physics in charm meson leptonic and semileptonic decays. Phys. Rev. D **91**(9), 094009 (2015). arXiv:1502.07488 [hep-ph]

22. G. Banelli, R. Fleischer, R. Jaarsma, G. Tetlalmatzi-Xolocotzi, Decoding (pseudo)-scalar operators in leptonic and semileptonic *B* decays. Eur. Phys. J. C **C78**(11), 911 (2018). arXiv:1809.09051 [hep-ph]

23. G. Banelli, R. Fleischer, R. Jaarsma, G. Tetlalmatzi-Xolocotzi, Probing lepton universality with (semi)-leptonic B decays. SciPost Phys. Proc. **1**, 013 (2019). arXiv:1812.05200 [hep-ph]

24. M. Tanaka, R. Watanabe, New physics in the weak interaction of $\bar{B} \to D^{(*)}\tau\bar{\nu}$. Phys. Rev. D **87**(3), 034028 (2013). arXiv:1212.1878 [hep-ph]

25. Y. Sakaki, M. Tanaka, A. Tayduganov, R. Watanabe, Testing leptoquark models in $\bar{B} \to D^{(*)}\tau\bar{\nu}$. Phys. Rev. D **88**(9), 094012 (2013). arXiv:1309.0301 [hep-ph]

26. L. Riggio, G. Salerno, S. Simula, Extraction of $|V_{cd}|$ and $|V_{cs}|$ from experimental decay rates using lattice QCD $D \to \pi(K)\ell\nu$ form factors. Eur. Phys. J. C **78**, 501 (2018). arXiv:1706.03657 [hep-lat]

27. L. Wolfenstein, Parametrization of the Kobayashi–Maskawa matrix. Phys. Rev. Lett. **51**, 1945 (1983). https://doi.org/10.1103/PhysRevLett.51.1945

28. A.J. Buras, M.E. Lautenbacher, G. Ostermaier, Waiting for the top quark mass, $K^+ \to \pi^+\nu\bar{\nu}$, $B_s^0 - \bar{B}_s^0$ mixing and CP asymmetries in B decays. Phys. Rev. D **50**, 3433–3446 (1994). https://doi.org/10.1103/PhysRevD.50.3433

29. A.J. Buras, Unitarity triangle: 2002 and beyond, 14th Rencontres de Blois on Matter—anti-matter asymmetry Chateau de Blois, France, June 17–22, 2002 (2002). arXiv:hep-ph/0210291 [hep-ph]

30. M. Tanabashi et al. (Particle Data Group), Review of particle physics. Phys. Rev. D **98**(3), 030001 (2018). https://doi.org/10.1103/PhysRevD.98.030001

31. C. Bouchard, L. Cao, P. Owen, Summary of the 2018 CKM working group on semileptonic and leptonic *b*-hadron decays. In: 10th International Workshop on the CKM Unitarity Triangle (CKM 2018) Heidelberg, Germany, September 17–21, 2018 (2019). arXiv:1902.09412 [hep-ex]

32. S. Aoki et al. (Flavour Lattice Averaging Group), FLAG Rev. **2019** (2019). arXiv:1902.08191 [hep-lat]

33. A.G. Akeroyd, Effect of $H^\pm$ on $D_s^\pm \to \mu^\pm\nu_\mu$ and $D_s^\pm \to \tau^\pm\nu_\tau$. Prog. Theor. Phys. **111**, 295–299 (2004). https://doi.org/10.1143/PTP.111.295

34. A.G. Akeroyd, F. Mahmoudi, Constraints on charged Higgs bosons from $D_s^\pm \to \mu^\pm\nu$ and $D_s^\pm \to \tau^\pm\nu$. JHEP **04**, 121 (2009). arXiv:0902.2393 [hep-ph]

35. A.G. Akeroyd, S. Recksiegel, Large enhancement of $D^\pm \to e^\pm\nu$ and $D_s^\pm \to e^\pm\nu$ in *R* parity violating SUSY models. Phys. Lett. B **554**, 38–44 (2003). https://doi.org/10.1016/S0370-2693(02)03293-8

36. M. Ablikim et al. (BESIII Collaboration), Observation of the leptonic decay $D^+ \to \tau^+\nu_\tau$. Phys. Rev. Lett. **123**(21), 211802 (2019). arXiv:1908.08877 [hep-ex]

37. C. Aubin et al. (Fermilab Lattice, MILC and HPQCD Collaborations), Semileptonic decays of D mesons in three-flavor lattice QCD. Phys. Rev. Lett. **94**, 011601 (2005). https://doi.org/10.1103/PhysRevLett.94.011601

38. V. Lubicz, L. Riggio, G. Salerno, S. Simula, C. Tarantino (ETM Collaboration), Scalar and vector form factors of $D \to \pi(K)\ell\nu$ decays with $N_f = 2 + 1 + 1$ twisted fermions. Phys. Rev. D **96**(5), 054514 (2017). arXiv:1706.03017 [hep-lat]

39. V. Lubicz, L. Riggio, G. Salerno, S. Simula and C. Tarantino (ETM Collaboration), Tensor form factor of $D \to \pi(K)\ell\nu$ and $D \to \pi(K)\ell\ell$ decays with $N_f = 2+1+1$ twisted-mass fermions. Phys. Rev. D **98**(1), 014516 (2018). arXiv:1803.04807 [hep-lat]

40. M.A. Ivanov, J.G. Körner, J.N. Pandya, P. Santorelli, N.R. Soni, C.T. Tran, Exclusive semileptonic decays of D and D_s mesons in the covariant confining quark model. Front. Phys. (Beijing) **14**(6), 64401 (2019). arXiv:1904.07740 [hep-ph]

41. R.N. Faustov, V.O. Galkin, X.W. Kang, Semileptonic decays of *D* and D_s mesons in the relativistic quark model (2019). arXiv:1911.08209 [hep-ph]

42. K.C. Bowler et al. (UKQCD Collaboration), An 'improved' lattice study of semileptonic decays of D mesons. Phys. Rev. D **51**, 4905–4923 (1995). https://doi.org/10.1103/PhysRevD.51.4905

43. Y.-L. Wu, M. Zhong, Y.-B. Zuo, $B_{(s)}, D_{(s)} \to \pi, K, \eta, \rho, K^*, \omega, \phi$ transition form factors and decay rates with extraction of the CKM parameters $|V_{ub}|, |V_{cs}|, |V_{cd}|$. Int. J. Mod. Phys. **A21**, 6125–6172 (2004). https://doi.org/10.1142/S0217751X06033209

44. M. Fael, T. Mannel, K.K. Vos, The heavy quark expansion for inclusive semileptonic charm decays revisited. JHEP **12**, 067 (2019). arXiv:1910.05234 [hep-ph]

45. H.-B. Fu, X. Yang, R. Lü, L. Zeng, W. Cheng, X.-G. Wu, The $D \to \rho$ transition form factors within the QCD light-cone sum rules and the D-meson semileptonic decays $D^0 \to \rho^-e^+\nu_e$ and $D^+ \to \rho^0e^+\nu_e$ (2018). arXiv:1808.06412 [hep-ph]

46. W.Y. Wang, Y.-L. Wu, M. Zhong, Heavy to light meson exclusive semileptonic decays in effective field theory of heavy quarks. Phys. Rev. D **67**, 014024 (2003). https://doi.org/10.1103/PhysRevD.67.014024